NIGHTTIME NITRATE RADICAL OXIDATION OF BIOGENIC VOLATILE ORGANIC COMPOUNDS NEAR HOUSTON, TX

A Thesis

by

JORDAN MAE MCCORMICK

Submitted to the Office of Graduate and Professional Studies of
Texas A&M University
In partial fulfillment of the requirements for the degree of

MASTER OF SCIENCE

Chair of Committee,	Don Collins
Committee Members,	Sarah Brooks
	Daniel Thornton
Head of Department,	Ping Yang

August 2017

Major Subject: Atmospheric Sciences

ABSTRACT

During the summer of 2016, measurements of secondary aerosol formation and resulting particle growth rates were made using the Captive Aerosol Growth and Evolution (CAGE) environmental chambers. The chambers were employed at a site in the WG Jones States Forest north of Houston, TX, where reaction of biogenic volatile organic compounds (BVOC) such as isoprene and the monoterpenes is enhanced through interaction with anthropogenic primary and secondary pollutants from the Houston area. The CAGE chambers are designed to study secondary aerosol production under ambient conditions. Monodisperse particles are intermittently injected into the chambers and their growth monitored to quantify time- and day-dependent aerosol production rate. Daytime particle growth can be attributed to photochemistry driven by UV radiation during peak solar intensity hours. After sunset, a distinct second period of growth occurs. This growth period is largely due to reaction of the nitrate radical (NO_3·) with isoprene and the monoterpenes. The nitrate radical is rapidly photolyzed during the day and does not become important in secondary aerosol production until nighttime. Oxidant and trace gas concentration measurements combined with nocturnal growth rates shows that nighttime NO_3· chemistry is significant for secondary aerosol formation at this site.

CONTRIBUTORS AND FUNDING SOURCES

Contributors

This work was supervised by a thesis committee consisting of Dr. Don Collins, advisor, and Dr. Sarah Brooks of the Department of Atmospheric Sciences and Dr. Daniel Thornton of the Department of Oceanography.

The data for Section 4.3 and 4.4 was compiled by Matt Erickson from the University of Houston. All other work conducted for the thesis was completed by the student independently.

Funding Sources

Graduate study was supported by funding from Sandia National Laboratory.

TABLE OF CONTENTS

Page

LIST OF FIGURES

Page

Page

Page

LIST OF TABLES

Page

1. INTRODUCTION AND LITERATURE REVIEW

In the troposphere, free radicals play an important role as oxidants. Traditionally, tropospheric oxidation has been largely discussed in terms of the hydroxyl radical (OH), peroxy radical (HO_2), and ozone (O_3). These photochemically produced oxidants have high concentrations during the day. During the last 50 years, the understanding of nighttime oxidants has greatly increased. Nighttime oxidants can have fast reactions that may be as fast, if not more so, than their daytime counterparts. Nitrate radical ($NO_3\cdot$) is one such nighttime oxidant.

The nitrate radical was first detected in the troposphere by Platt et al. (1980) and Noxon et al. (1980). Platt et al. used long path differential optical absorption spectroscopy (DOAS) in the Los Angeles basin. $NO_3\cdot$ was measured up to 355 parts per trillion (ppt), with peaks one hour after sunset (Platt et al., 1980). Noxon et al. used moonlight absorption measurements of nighttime $NO_3\cdot$. In their study, higher levels were observed later in the night compared to those measured shortly after sunset. These two studies spurred several measurements of the $NO_3\cdot$ in both polluted and clean background air (1980).

Nitrate radical chemistry in the atmosphere is explained in detail by several publications (e.g., Platt et al., 1980, 1981; Heikes and Thompson, 1983; Wayne et al., 1991; Heintz et al., 1996). The dominant source of nitrate radicals in the troposphere is the reaction of NO_2 with O_3,

$$NO_2 + O_3 \rightarrow NO_3\cdot + O_2 \qquad (1)$$

$NO_3\cdot$ is lost through reactions with NO_2 (2), its self-reaction (3), and its thermal decay (4):

$$NO_3\cdot + NO_2 \rightarrow NO + NO_2 + O_2 \quad (2)$$

$$NO_3\cdot + NO_3\cdot \rightarrow NO_2 + NO_2 + O_2 \quad (3)$$

$$NO_3\cdot + M \rightarrow NO + O_2 + M \quad (4)$$

A rapid loss mechanism is the gas phase reaction with NO:

$$NO_3\cdot + NO \rightarrow NO_2 + NO_2 \quad (5)$$

This leads to typical daytime degradation frequencies of 0.1 – 1 s^{-1} at NO levels of 0.13 – 1.3 ppb (Geyer et al., 2001).

In the absence of light, relevant quantities of N_2O_5 and $NO_3\cdot$ can be formed (6):

$$NO_2 + NO_3\cdot \leftrightarrow N_2O_5 \quad (6)$$

Due to the rapid photolysis of $NO_3\cdot$ and typically lower NO at night, $NO_3\cdot$ is highest after sunset (Geyer et al., 2001; von Kuhlmann et al., 2004; Horowitz et al., 2007; Xie et al., 2013). Table 1 shows the reactions involved in tropospheric nitrate radical chemistry and the associated rate constants.

Platt et al. used optical absorption spectroscopy again to measure $NO_3\cdot$**,** but focused on the diurnal variation and possible sinks (1981). They found that at night, measurements rose to a maximum of 280 ppt in the early morning, but within 30 minutes of sunrise $NO_3\cdot$ dropped below the detection limits. Nighttime $NO_3\cdot$ and peroxy radical (HO_2) concentrations were measured in Black Forest, Germany by Mihelcic et al., (1993). Nitrate radical levels were in the range of 0 – 10 ppt, while organic peroxy

radical concentrations reached 40 ppt. These measurements suggest an anticorrelation between NO_3· and RO_2 at night (Mihelcic et al., 1993).

In 1990 Smith et al. used DOAS to measure NO_3· in the San Joaquin valley in central California. They also found NO_3· highest an hour after sunset with maximums of 31 ppt. Heintz et al. also used DOAS to measure nitrate radical, but at a rural site near the Baltic Sea. Measurements were taken over 14 months and an average nighttime NO_3· of 7.8 ppt was determined.

Once discovered in the atmosphere, NO_3· was recognized as an important atmospheric oxidant with the potential to serve as a large sink for biogenic volatile organic compounds (BVOC). It was in 1984 when Winer et al. showed that NO_3· reacts rapidly with biogenically emitted organic compounds such as dimethyl sulfide (DMS), isoprene, and several monoterpenes. They measured the rate constants for the reaction of NO_3· with a large number of organics and found rapid reaction rates ranging from ~ 5 X 10^{-13} cm^3 s^{-1} to 1 X 10^{-12} cm^3 s^{-1} (Winer et al., 1984). The lifetimes of DMS, isoprene, and selected monoterpenes for the reactions with O_3, OH, and NO_3· were compared. In clean atmospheres, the lifetime with nighttime NO_3· was much shorter than O_3 and only slightly longer than OH for all compounds. In moderately polluted atmospheres, the lifetimes of all compounds due to nighttime NO_3· were much shorter than due to O_3 and OH (Winer et al., 1984).

Table 1. Rate constants of the reactions involved in tropospheric nitrate radical chemistry adapted from Geyer et al., 2001.

Reaction	***k(T)***
(1) $NO_2 + O_3 \rightarrow NO_3\cdot + O_2$	2.4×10^{-17} $cm^3\ s^{-1}$
(2) $NO_3\cdot + NO_2 \rightarrow NO + NO_2 + O_2$	5.7×10^{-16} $cm^3\ s^{-1}$
(3) $NO_3\cdot + NO_3\cdot \rightarrow NO_2 + NO_2 + O_2$	1.7×10^{-16} $cm^3\ s^{-1}$
(4) $NO_3\cdot + M \rightarrow NO + O_2 + M$	1.4×10^{-4} cm^3
(5) $NO_3\cdot + NO \rightarrow NO_2 + NO_2$	2.7×10^{-11} $cm^3\ s^{-1}$
(6) $NO_3\cdot + NO_2 + M \rightarrow N_2O_5 + M$	1.3×10^{-12} $cm^3\ s^{-1}$
$N_2O_5 + M \rightarrow NO_3\cdot + NO_2 + M$	1.3×10^{-2} cm^3

Lifetimes of $NO_3\cdot$ in rural environments can be very short due to the fast reactions of $NO_3\cdot$ with BVOC. This makes detecting VOC and $NO_3\cdot$ simultaneously in biogenic regions difficult. To overcome this obstacle several studies have inferred $NO_3\cdot$ levels and its role in processing BVOC using observational analysis and supporting modeling. The decay of isoprene after sunset has been of particular interest.

Several box model simulations could not completely explain the short lifetime of isoprene at night by the $NO_3\cdot$ radical (Biesenthal et a., 1998; Starn et al., 1998; Hurst et al., 2001; Steinbacher at al., 2005). These studies found that either $NO_3\cdot$ had no significant influence on isoprene decay or that $NO_3\cdot$ oxidation was only significant after the majority of isoprene had already decayed. Indirect conclusions about the role of

NO_3· in BVOC processing have been made through these studies, but direct measurements of these compounds are still needed to confirming these results.

The 1990 ROSE program measured BVOC above the canopy level in a plantation in Alabama (Goldan et al., 1995). These measurements were used to infer a nighttime NO_3· mixing ratio of 0.2 ppt and a lifetime of only 7 s due to high levels of monoterpenes. Gas reactions with NO_3· and O_3 could not account for the 4 h decay time of isoprene after sunset. The α-/ β-pinene ratio at night was found to be consistent with known NO_3· and O_3 chemistry (Goldan et al., 1995).

A field study was conducted at a Mediterranean eucalyptus forest in 1994 by Gölz and Platt. DOAS measurements of NO_2 and O_3 were used to determine NO_3· production at the site, but NO_3· was also directly measured. Though high NO_3· production was observed, NO_3· remained below 6 ppt. It was believed that reactions with olefins were the dominant sink, especially with the sufficiently high olefin concentrations that were observed (Gölz and Platt, 2001). Another similar analysis was done in Scandinavia by Ljungström and Hallquist (1996). They calculated NO_3· formation rates and concluded that nighttime urban loss of NO_3· is dominated by reaction with NO, but rural loss is likely dominated by reactive hydrocarbons. They also concluded that out of the hydrocarbons, the monoterpenes were the most active (Ljungström and Hallquist, 1996).

During the Berliner Ozone Experiment (BERLIOZ) campaign in 1998, simultaneous measurements of NO_3· and VOC were made. This allowed for one of the first assessments of the NO_3· budget in comparison to OH and O_3 (Geyer et al., 2001b).

Surface measurements found NO_3· to be above the detection limit (2.4 ppt) on 15 of 19 nights. A maximum of 70 ppt was observed with steady-state lifetimes ranging from 20 to 540 s. The significant losses of NO_3· were found to be its direct reaction with olefins, specifically the monoterpenes.

NO_3·, isoprene, and its oxidation products were measured in Nashville, TN as part of the 1999 Southern Oxidants Study (SOS) study (Stroud et al., 2002). NO_3· was measured by DOAS and had maximum mixing ratios of 100 ppt that were found to be anticorrelated with isoprene levels. Losses of isoprene in the early evenings were found to be attributed to reactions with NO_3·. During the Pacific 2001 Air Quality Study (PACIFIC 2001) maximum nighttime NO_3· levels of up to 50 ppt were found (McLaren et al., 2004). Simultaneous analysis of carbonyl compounds during the study found that only monoterpene oxidation products were enhanced in aerosol filters collected at night (Liggio and McLaren, 2003). Measurements of NO_3·, N_2O_5, isoprene and its oxidation products were measured in 2004 as part of the New England Air Quality Study (NEAQS) and the Atmospheric Research on Transport and Transformation (ICARTT) campaigns (Brown et al., 2009). A very clear anticorrelation between isoprene levels after dark and NO_3· mixing ratios were found. The loss frequencies of NO_3· were strongly correlated with the loss rate constant of NO_3· with isoprene reactions for isoprene lifetimes less than 20 min. It clearly showed that isoprene was the most important species determining the lifetime of NO_3·.

Numerous studies have also investigated the role of NO_3·+BVOC chemistry in more polluted areas. Brown and Stutz presented observations in Houston, TX (2010,

2011, 2013). It was found that 50% of the NO_3·+BVOC reactions in Houston due to NO_3·+isoprene reactions, with the other VOC emitted by industrial sources. It was found that in Houston, heterogeneous NO_3·/N_2O_5 chemistry plays a minor role. The nocturnal VOC oxidation by NO_3· dominates that by ozone. The nocturnal NO_3· formation rates were rapid and comparable to those of OH during the day (Brown et al., 2011).

NO_3· chemistry in marine, continental and urban originated air masses at a field site in southern Spain were compared by Crowley et al. (2011). All of the conditions showed NO_3·+BVOC reactions contributed to the overall NO_3· reactivity. This confirmed other observations that this chemistry is important where BVOC sources are present, no matter the environment.

Secondary organic aerosol (SOA) is an important source of aerosol mass. Approximately 70% of total global organic aerosol production is secondary (Hallquist et al., 2009). Formation mechanisms remain uncertain, but a large fraction of total organic aerosol is thought to originate from the oxidation products of BVOC emissions.

To produce condensable oxidation products, and thus form SOA, the precursor VOC generally needs to contain a minimum number of carbon atoms. This is due to the dependence on molecular weight and polarity for partitioning of the VOC products to the aerosol phase (Pankow and Barsanti, 2009). Such VOC include isoprene and monoterpenes. Isoprene (C_5H_8) is the globally dominant BVOC. It comprises ~50% of total global nonmethane VOC emissions by mass (Guenther et al., 2012). However, isoprene and its NO_3· oxidation products are quite volatile. Thus, isoprene has relatively low NO_3· SOA yields.

Several laboratory and theoretical studies have been done to measure the kinetics and gas-phase products of the isoprene-NO_3· reaction (Jay and Stieglitz, 1989; Barnes et al., 1990; Skov et al., 1992; Kwok et al., 1996; Berndt and Böge, 1997; Suh et al., 2001; Zhang et al., 2002; Fan et al., 2004). Many studies have identified C_5-nitrooxycarbonyl as the major first-generation gas-phase reaction product (Jay and Stieglitz, 1989; Skov et al., 1992; Kwok et al., 1996; Berndt and Böge, 1997). The yield for nitrate-containing compounds from the reaction of isoprene and NO_3· radicals can be as high as 80% (Barnes et al., 1990). Results from the ICARTT field campaign also suggest that ~50% of the total isoprene nitrate production occurs through the isoprene and NO_3· reactions (Horowitz et al., 2007). However, little is known beyond the formation of the first-generation products of this reaction. Isoprene nitrates and other first-generation products contain a carbon-carbon double-bond and further oxidation of these species will likely lead to low volatility products that can contribute to SOA formation at night (Ng et al., 2008).

Several laboratory studies using environmental chambers have been conducted to determine the importance of NO_3·-BVOC chemistry in nighttime SOA formation. The SOA mass yield was investigated using various BVOCs and batches of nitrate radical (Hallquist et al., 1999; Griffin et al., 1999; Splitter et al., 2006; Moldanova and Ljungstrom, 2000; Ng et al., 2008; Fry et al., 2009; Rollins et al., 2009; Perraud et al., 2010; Fry et al., 2014; Boyd et al., 2015; Nah et al., 2016). These experiments typically were conducted under conditions that focused only on first-generation oxidation. In the real atmosphere, further oxidation can continue to change SOA loadings. These chamber

studies found that the monoterpenes are efficient sources of SOA with the exception of α-pinene. A much larger carbonyl yield is produced from α-pinene oxidation instead of the typical organic nitrates. There have not been as many chamber studies investigating isoprene oxidation as the monoterpenes, but those that have been done have shown variable SOA yields.

Evidence of aerosol formation from NO_3·-BVOC chemistry, during both daytime and nighttime, has been provided by previous field studies (McLaren et al., 2004; Iinuma et al., 2007; Fuentes et al., 2007; Brown et al., 2009, 2013; Rastogi et al., 2011; Rollins et al., 2012, 2013). The field experiment conducted by Brown et al., (2013) is of particular interest. Flight measurements were done in the summer of 2006 in Houston, TX. The vertical distribution of nocturnal trace gases was measured and the data showed that organic aerosol was enhanced in the boundary layer at night. The concentration of organic aerosol observed were in excess of those attributed to primary emissions. Results from this field experiment imply that in Houston the BVOCs+NO_3· reactions are a source of nocturnal SOA.

There has been extensive research done on the nighttime oxidation of BVOCs by NO_3·, both in situ and in laboratory studies. Chamber studies have allowed for the observation of these chemical reactions and the production of SOA in a controlled setting. Field studies have allowed for proof of SOA production in the atmosphere, but are unable to directly observe the growth of the particles due to NO_3·-BVOC chemistry.

Texas A&M University, along with Baylor University, Rice University, University of Houston and Sandia National Laboratories, conducted a field campaign in

the late summer of 2016 between August and October. Captive Aerosol Growth and Evolution (CAGE) chambers developed in the research group of Dr. Don Collins in conjunction with trace gas analyzers from University of Houston, an aerosol mass spectrometer (AMS) from Rice University and a proton transfer reaction – mass spectrometer (PTR-MS) from Baylor University were deployed to a field site north of Houston. Trace gases and various hydrocarbons were measured during this time. The CAGE chambers allowed for atmospheric reactions with the surrounding ambient air while still conducting controlled aerosol formation experiments. The goal of the analysis of this data is to better understand nighttime nitrate radical reactions with isoprene and monoterpenes. This is done through directly observing SOA formation by measuring the production rate associated with this formation.

2. INSTRUMENTATION

2.1. CAGE Chambers

The Captive Aerosol Growth and Evolution (CAGE) chambers are cubic meter environmental chambers, shown in Figure 1. These two identical chambers allow for controlled experiments while still supporting natural atmospheric reactions with the surrounding ambient air. The ambient air flow system creates a method to constantly introduce new ambient air into the chambers. The chambers are UV transmitting, allowing photolysis of particles present in the chambers. Photolysis driven daytime reactions can proceed without interruption inside of the chambers.

Figure 1. CAGE chambers during the field campaign.

The skeleton of the chambers is made from stainless steel and is comprised of a long axle with five large rings attached to it. The stainless steel is wrapped in Teflon tape to prevent heating and to allow for UV reflection. The end rings have thick polytetrafluoroethylene (PTFE) material wrapped around the rings creating a channel. These channels are wrapped in Teflon surrounded wires. One end ring has a fluorinated ethylene propylene (FEP) end sheet sealed around the axle and the channel. The other end ring has a gas permeable expanded polytetrafluoroethylene (ePTFE) membrane sealed around the axle and the channel. Over the entire chamber is a cylindrical heat sealed FEP bag that is stretched over both channels and sealed against them with a clamped wire system. The membrane side of the chamber has two filters attached to a FEP tube that extends through the membrane and into the chamber as shown in Figure 2. This allows for the replacement of air inside the chamber as air is being sampled and for venting of air inside as particle-containing flows are injected. The chamber's axle has an open tube running through it with ports on either end. A port on the axle, located inside of the chamber, allows for sampling and injection.

Figure 2. Picture of FEP tube extending inside of the chamber. This allows for the replacement of filtered air inside the chamber during sampling.

The chambers are set inside of large rectangular powder coated stainless steel frames covered on all sides by UV transmitting acrylic panels. An PTFE gasket covering the bottom acrylic panel reflects visible and UV radiation into the chambers to offset attenuation through the top and side acrylic panels and the FEP chamber walls. The axle is secured to steel bearings located inside the frame. A sprocket secured to one end of the axle is connected by a chain to a small motor that allows the chambers to rotate at around 1 rpm. Figure 3 shows the ambient air flow around the chamber. Air is pulled in from the top and flows past the permeable membrane. It then flows under the chamber and is pulled out by a blower that is attached to the bottom acrylic panel.

Figure 3. Ambient air flow system inside the chamber enclosures. Ambient air is pulled by a blower on the bottom through a hole in the top. The air path is shown in red.

2.2. Scanning Mobility Particle Sizer

Particles inside the chambers were measured by a scanning mobility particle sizer (SMPS). Figure 4 shows a schematic of the SMPS set-up along with the atomizer system used for injection. Samples are extracted from the membrane side of the chamber, while particles are injected into the opposite end. A three-way valve on the outside of the SMPS cart switches between sampling chamber air and ambient air. The particles are then dried and charge neutralized by a Nafion tube and a soft x-ray neutralizer. The particles are then sized by the differential mobility analyzer (DMA) in the SMPS, and

are finally counted by the condensation particle counter (CPC). The SMPS size range was from 0.012 μm to 0.6 μm, and it cycled through 75 size bins in 60 seconds.

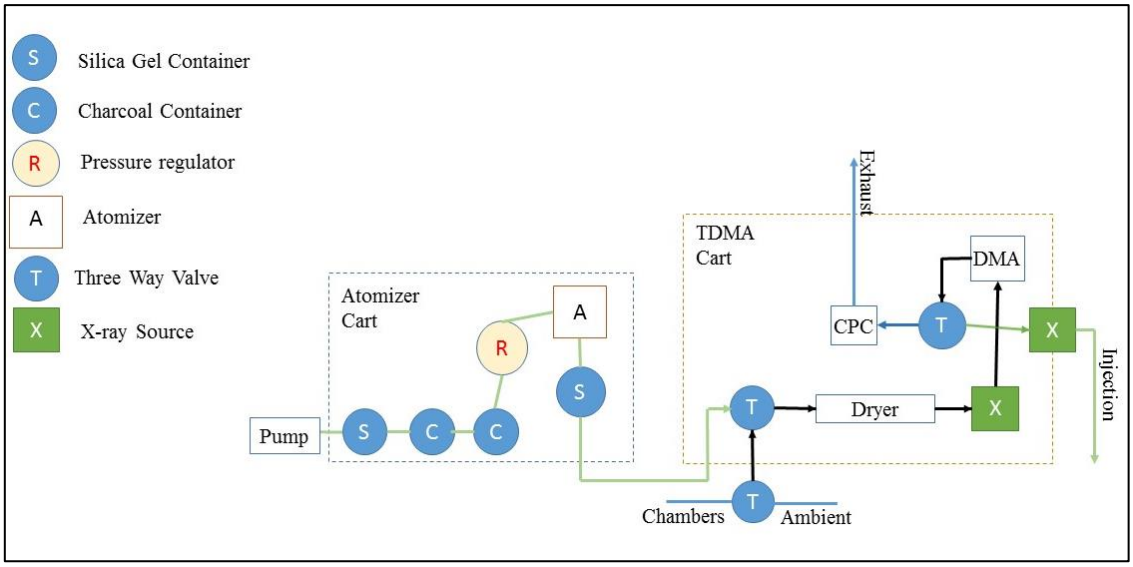

Figure 4. Schematic of SMPS and Atomizer set up.

A mode of ~300 nm ammonium sulfate particles is injected into the chambers automatically when the surface area concentration falls below 40 μm^2 cm^{-3}. Ammonium sulfate particles are used due to their common usage in environmental chamber experiments which allows for easier comparison, but also because they are common inorganic particles naturally found in the atmosphere. The compressed air used for the atomizer is scrubbed through a silica gel container and two charcoal containers. The generated aerosol is size classified by the DMA in the SMPS system, neutralized by a soft x-ray neutralizer and then injected into the chamber. Injection times range from 5 to

15 min depending on the desired increase in chamber concentration and the particle size injected.

Injecting these ammonium sulfate particles resulted in a trackable mode observed inside of the chamber. The modes that were tracked for data analysis were the smaller particle modes evident in the number concentration distribution. Typically the 70 nm mode was tracked. The larger particle modes were automatically injected to maintain a stable surface area concentration. Figure 5 shows example number and surface area distributions that contained trackable modes. As the particles age the peak diameter increases while the concentration decreases. This is evident in the number concentration distribution. Eventually the concentration decreases to the point where the mode is lost to the background noise.

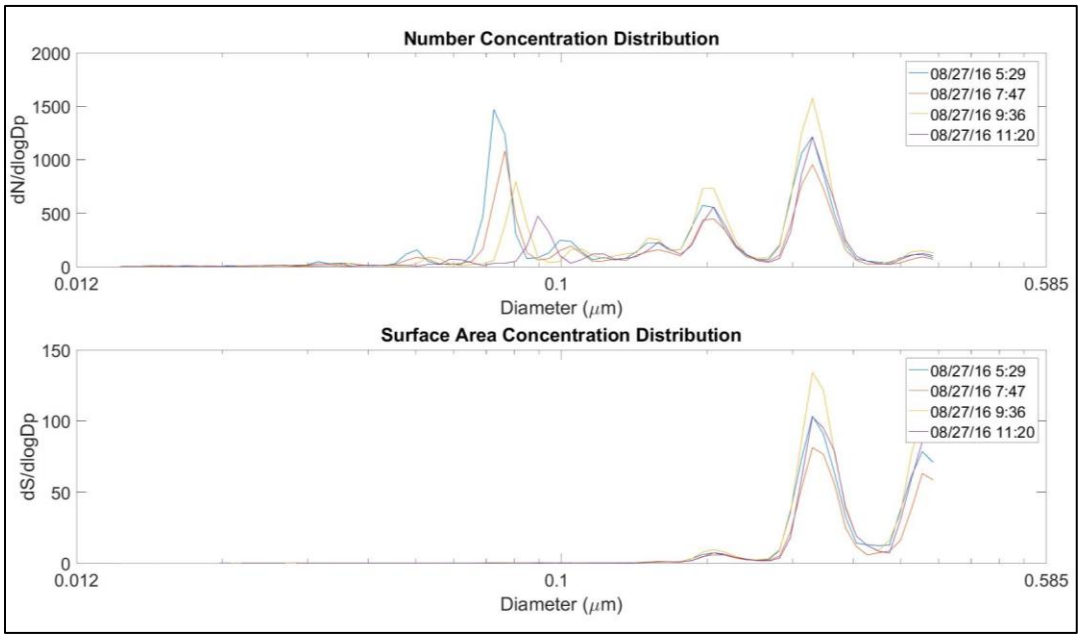

Figure 5. Number distribution and surface area distribution of particles sampled from the chambers at different times.

3. METHODOLOGY

A field campaign was conducted from August 2016 to mid-October 2016 at WG Jones State Forest in Conroe, Texas. The site is located 65 km north of Houston, and was chosen due to its relatively rural location surrounded by trees. The primary types of trees in WG Jones State Forest are pine trees. The CAGE chambers were used with an AMS from Rice University, a PTR-MS from Baylor University, and trace gas analyzers from University of Houston. Sandia National Laboratories coordinated this field campaign, and conducted their own experiments approximately once a day. While Sandia was conducting their own experiments, the SMPS still sampled from the chambers.

To minimize shading, the CAGE chambers were placed away from any trees or structures and were oriented with the membrane side facing north. The membrane (sample extraction) sides of the chambers faced the trailer with the SMPS inside to minimize the sample tubing length. Underneath each chamber was a three-way automated valve that directed sample or injected aerosol flows into one of the two chambers. Figure 6 shows a schematic of the chamber and trailer set up. Chamber A was located on the left while chamber B was located on the right. Each SMPS measurement lasted 312 seconds. Ambient air was sampled four consecutive times. Chamber A was then sampled from followed by chamber B. This resulted in around a half hour time span between each chamber sample. The surface area concentration was typically maintained by injecting 300 nm particles. During times when Sandia was conducting experiments

200 nm particles were injected instead to minimize interference with their optical detection of bioparticles.

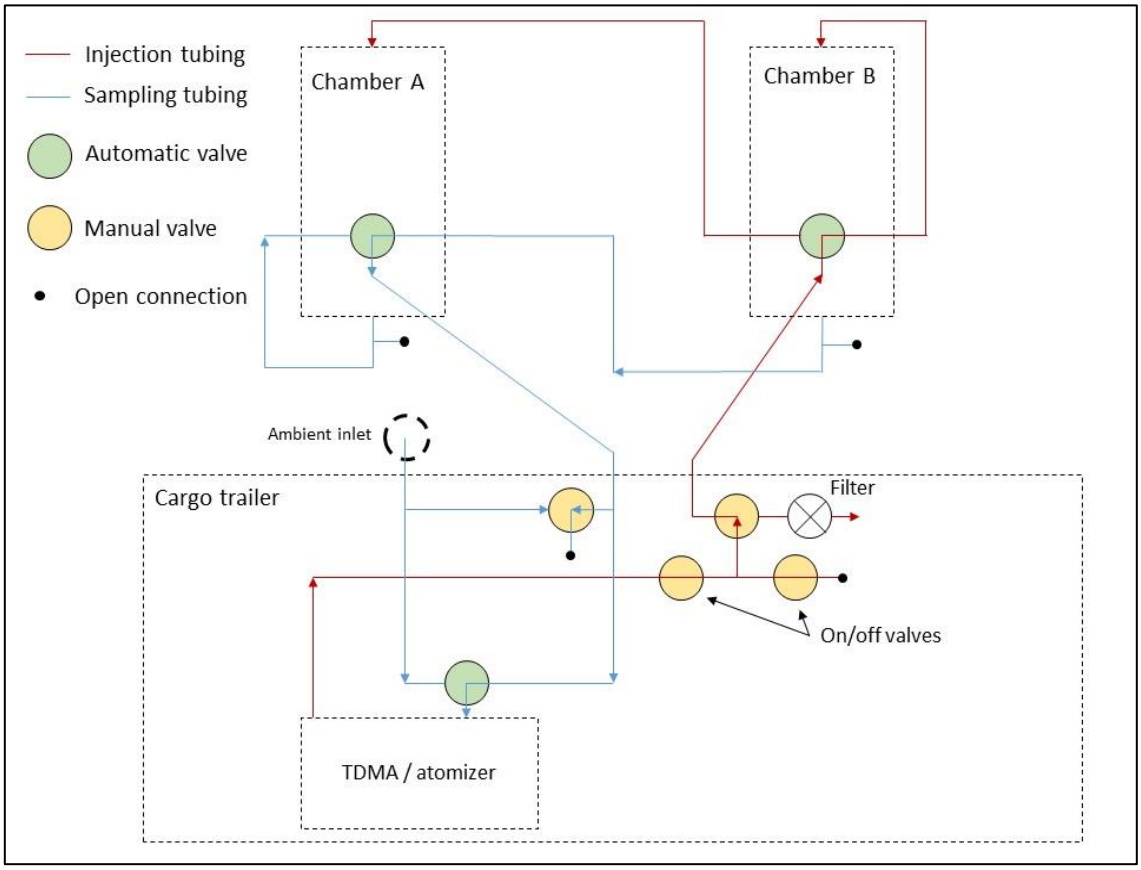

Figure 6. Schematic of chamber and trailer set up during the field campaign.

The trace gas analyzers, the AMS and the PTR-MS were located in a trailer to the east of the chambers. The ambient air line for the trace gas analyzers, the AMS, and the PTR-MS was located close to the instruments and was approximately 20 feet high. The SMPS ambient air line was located outside of the trailer and was also approximately

20 feet high. Trace gas analyzers measured O3, CO, NO, NO2, and SO2 from surrounding ambient air every minute. The PTR-MS measured selected m/z every minute and that data was averaged over longer time intervals as needed.

The CAGE chambers were used almost continuously from August 25th 2016 until October 14th 2016. PTR-MS data was collected from August 19th 2016 until September 22nd 2016. The trace gas analyzer data and the AMS data was collected from August 12th 2016 until September 21st 2016. Between September 9th and September 12th, the trace gas analyzers sampled from inside of both chambers to confirm that the concentrations of gases inside the chambers were consistent with the surrounding ambient air.

4. DATA ANAYLSIS

4.1. Meteorological Conditions

Meteorological parameters were not taken directly at the site, but instead at a weather station approximately one mile northwest of the field site. Figure 7 shows the various meteorological parameters collected.

The average temperature during the field campaign was 25°C. The daily highs were often in the 90s, while the daily lows were typically in the 20s. The relative humidity during the field campaign was almost always above 50% and often times near 100%. The average wind speed was around 6 km per hour. The wind direction was typically either from the Southeast or from the Northwest.

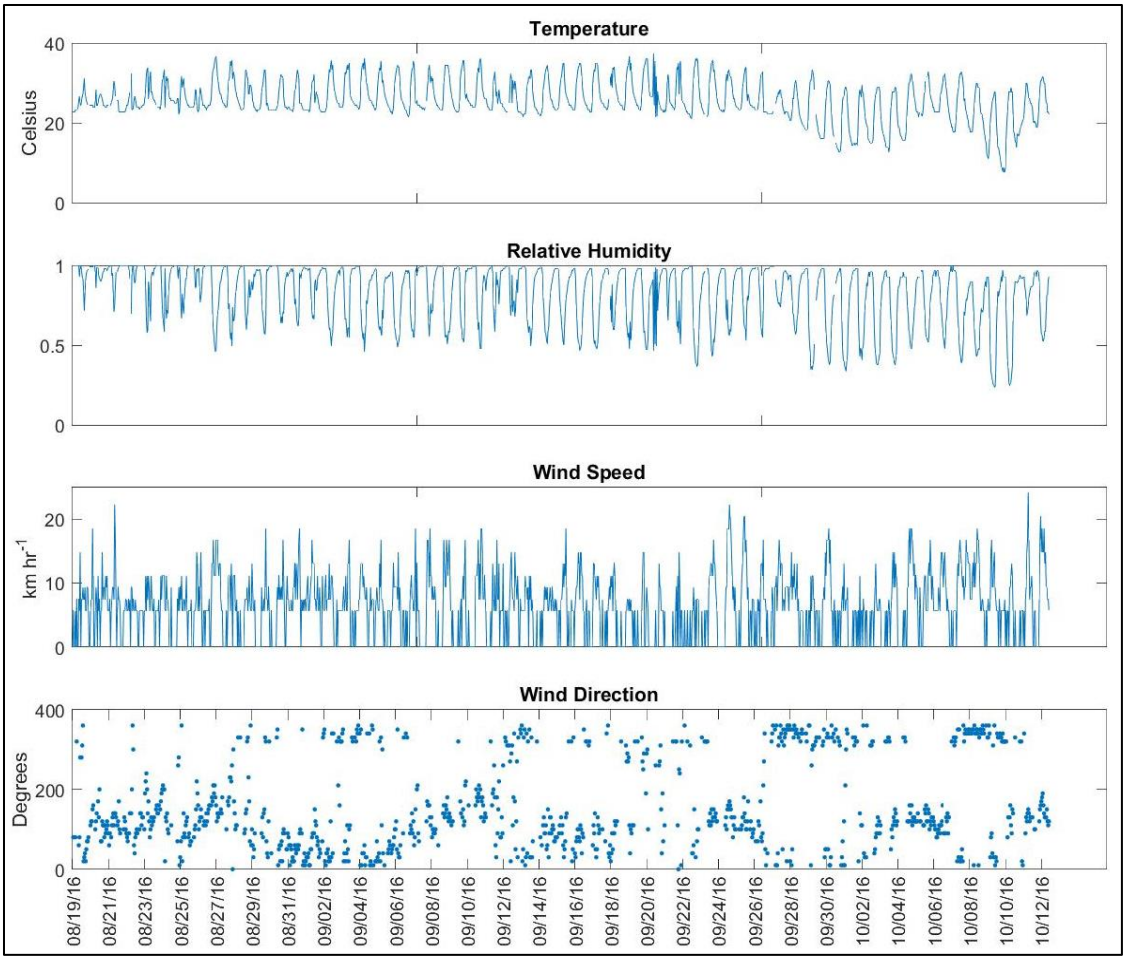

Figure 7. Hourly averaged meteorological parameters collected from weather station northwest of the field campaign

Figure 8 shows the daily precipitation during the field campaign. Precipitation exceeded 0.1 cm on 14 days. On days that it did rain, condensation often lingered in the CAGE enclosures for a few hours after the rain ended. This may have inhibited particle growth and this possibility is explored later in the analysis.

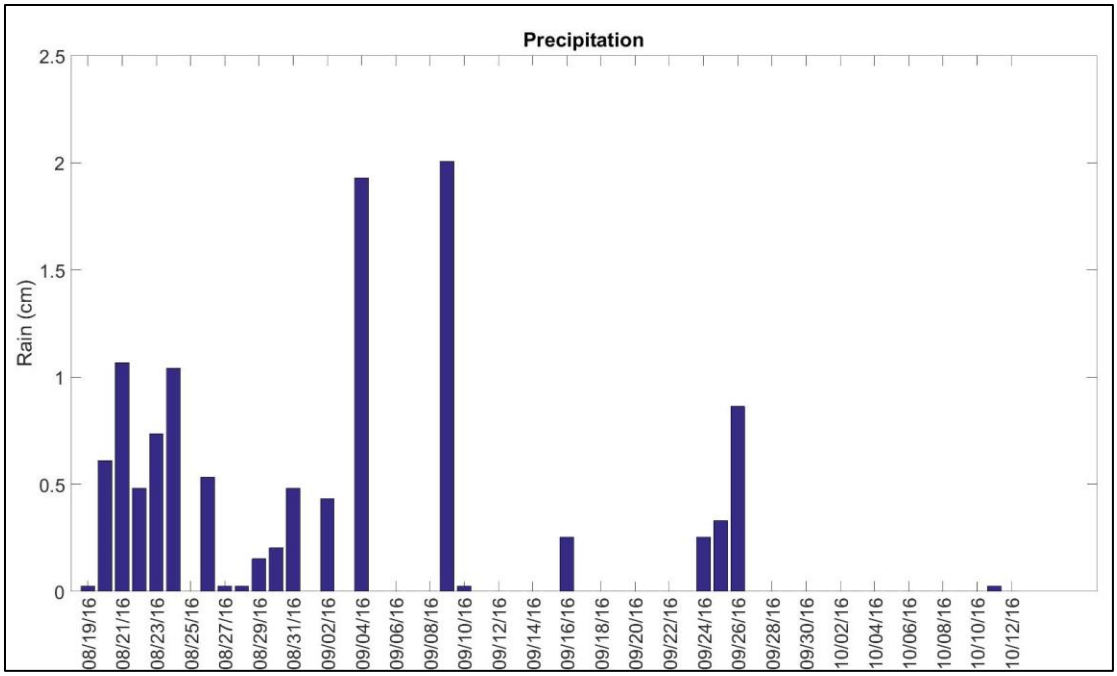

Figure 8. Total precipitation amount in inches collected from weather station northwest of the field campaign.

4.2. CAGE Chamber Data

Chamber data was collected every half hour. The parameters that were resolved are peak aerosol diameter and aerosol concentration. The peak aerosol diameter ranged from 13 nm to 175 nm. Modes were tracked until the peak was lost to the background noise. Often times as one peak was ending, another nucleation event started. This caused two peaks to be present at the same time. Figure 9 shows the growth in diameter for a typical tracked mode.

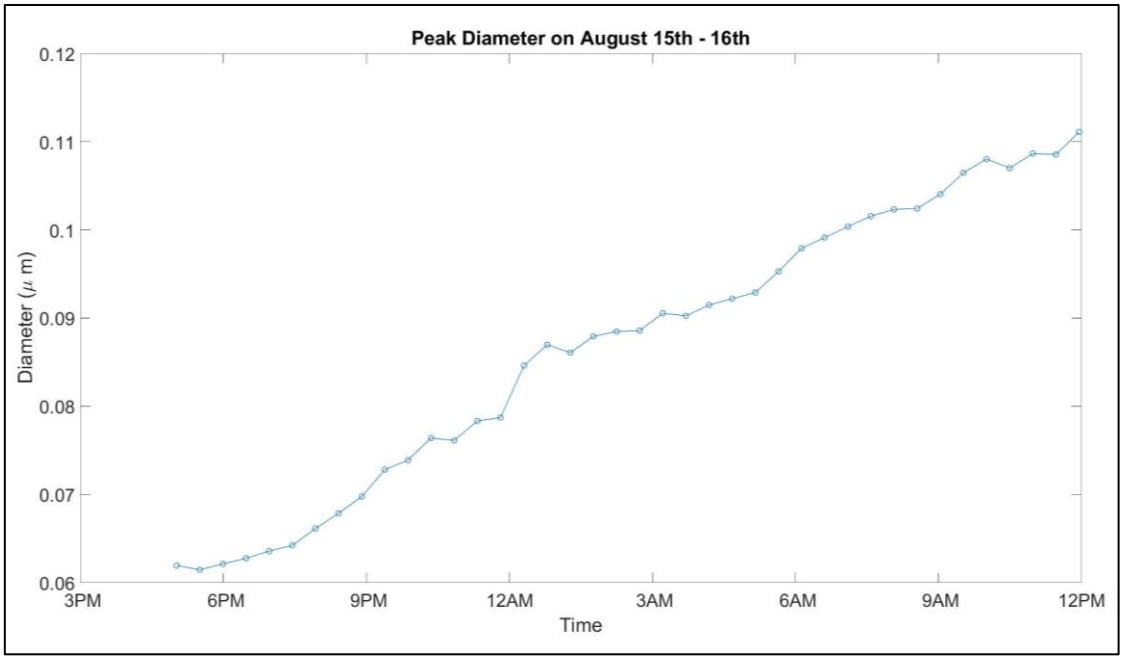

Figure 9. Peak diameter growth on the night of August 15th 2016

As peak particle diameter increases, the concentration of particles decreases. Figure 10 shows the decrease in concentration during the same time frame as the previous figure. Most modes decreased in a non-linear way and the concentration decreasing trend was caused by particles combining together to grow.

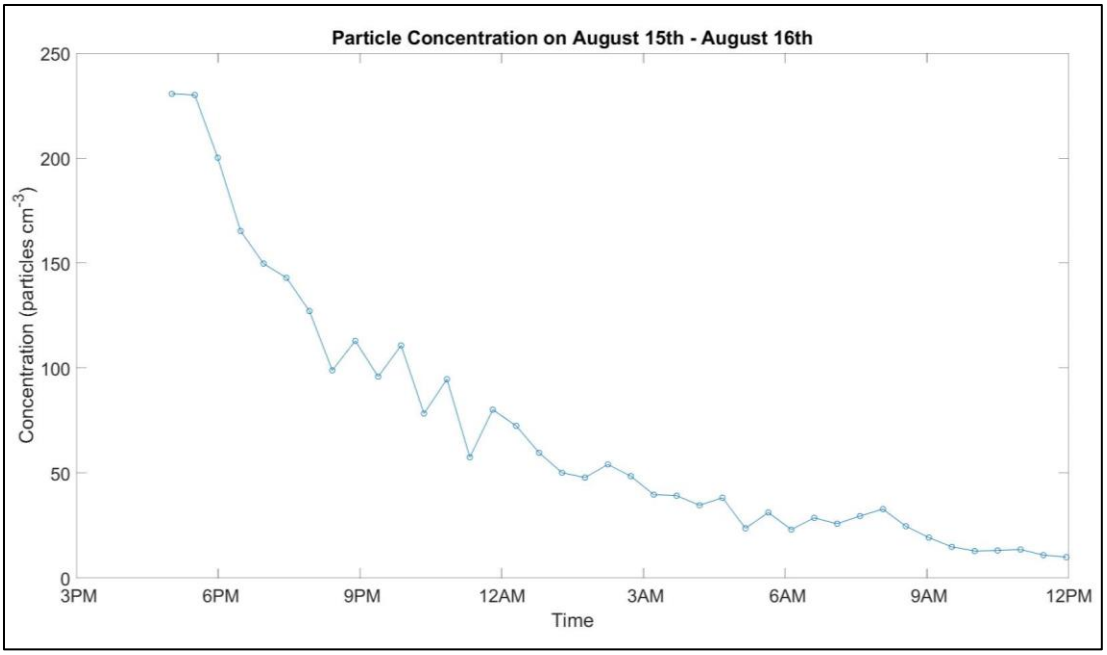

Figure 10. Particle concentration during night of August 15th 2016.

Growth rate was then determined using the measurement time and the peak diameter:

$$\frac{\mathrm{dy}}{\mathrm{dx}} = \frac{\Delta \mathrm{diameter}}{\Delta \mathrm{time}} = \frac{\mathrm{nm}}{\mathrm{hr}} \tag{7}$$

The particle growth rate over the same time frame as in Figure 8 and Figure 9 is shown in Figure 11. Growth rate varied greatly by time of day, and there were many hours where the particles shrunk. During the day, the peak growth rates were highest one or two hours after sunrise due to a shallow boundary layer and a buildup of VOCs.

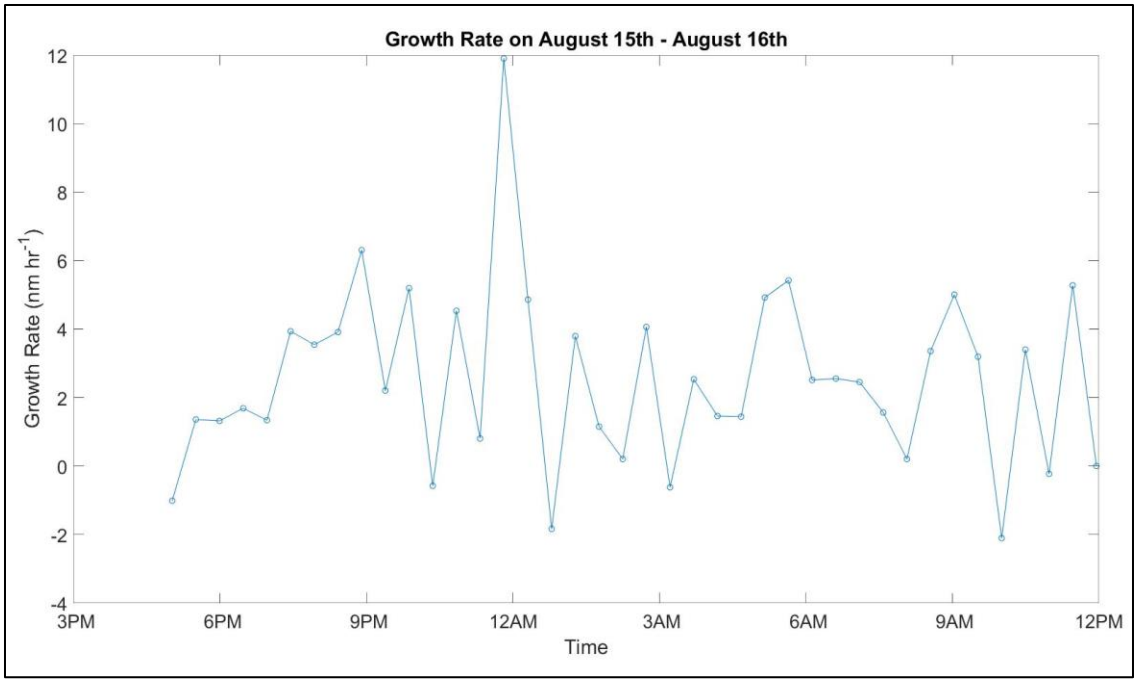

Figure 11. Calculated growth rate of particles during the evening of August 15th 2016.

Growth rates during the times that all instruments were collecting data are shown in Figure 12. Maximum growth rates were typically observed 1-2 hours after sunset and 1-2 hours after sunrise.

Nighttime growth rates were typically highest right after sunset and gradually decreased until sunrise, shown in Figure 13. Between sunset and midnight, growth rates were always higher than those between midnight and sunrise. Negative growth rates were occasionally observed, but often only after midnight.

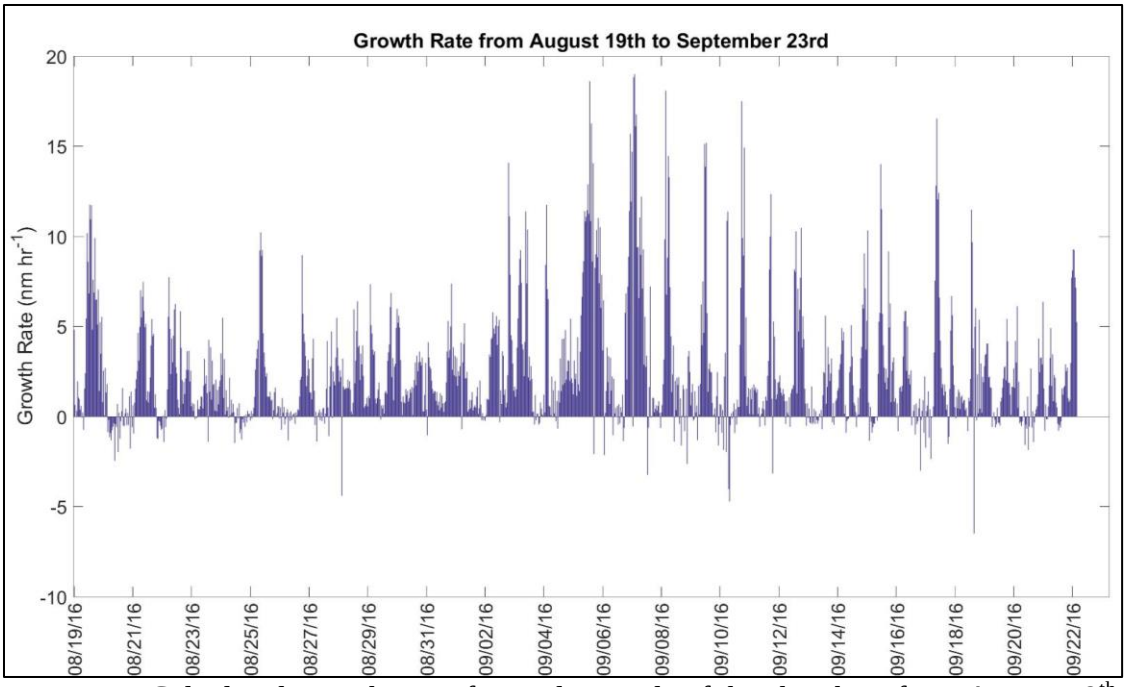

Figure 12. Calculated growth rate of particles inside of the chambers from August 19th 2016 to September 22nd 2016

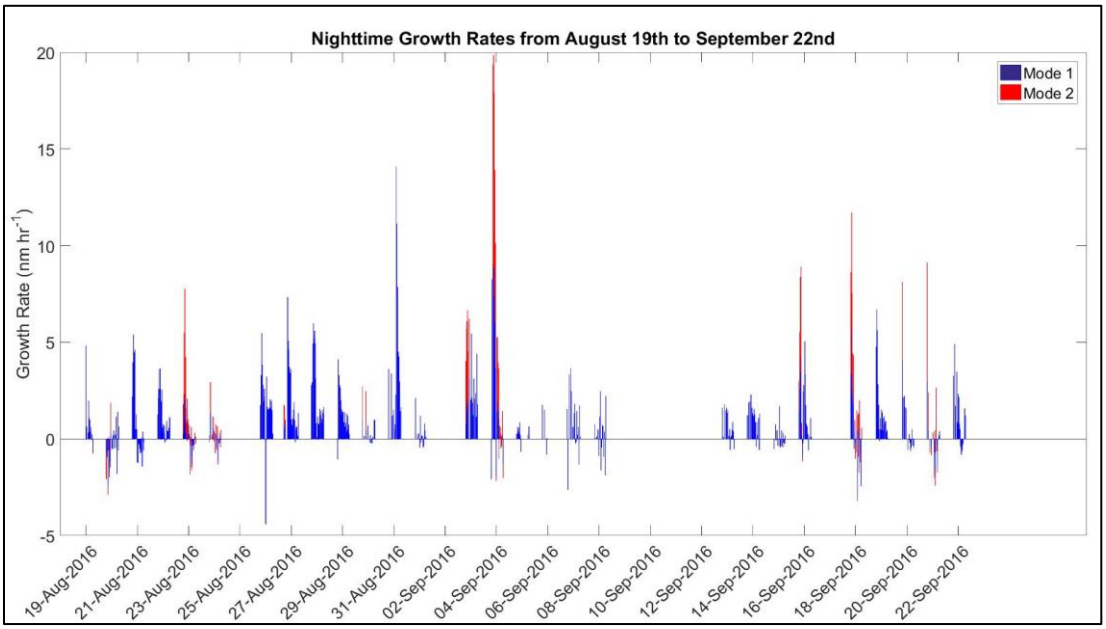

Figure 13. Growth rates of particles only between the hours of 19:00 CDT and 7:00 CDT. During times of multiple modes the growth rates are in different colors. Data weren't collected between September 9th and September 12th.

4.3. Trace Gas Analyzer Data

Trace gas analyzer data was averaged over every minute with the time stamp reflecting the beginning of the averaging period. Data was collected continuously between August 12th and September 22nd. Starting on September 9th at 16:20 until September 12th at 1:35 the trace gas analyzers sampled from the CAGE chambers. This was done to determine if the concentrations observed in the chambers resembled those observed in the surrounding ambient air.

Matthew Erickson from University of Houston calibrated both the trace gas analyzers and the PTR-MS and processed both sets of data. The trace gases that were measured are O_3, NO, NO_2, NO_y, SO_2, and CO. Table 2 shows the detection limits and the uncertainty of these measurements.

Table 2. Trace gases measured including the detection limits and uncertainty of the trace gas analyzer.

Gas	Detection Limit (ppbv)	Uncertainty (%)
O_3	2.15	4
NO	0.011	4
NO_2	0.044	7.7
NO_y	0.092	4.1
SO_2	0.11	4.4
CO	N/A	4

4.3.1. Ozone

Figure 14 shows the measured ozone averaged every minute during the field campaign. The O_3 ranged from 2 ppb to 69 ppb. The average over the field campaign was 20 ppb.

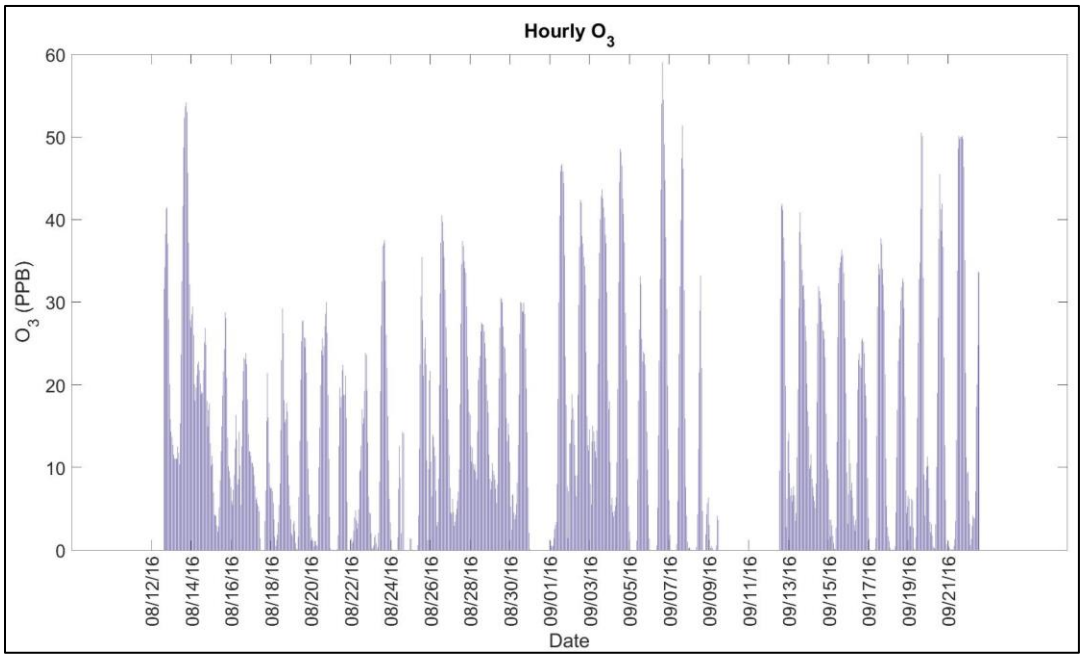

Figure 14. Ozone averaged every minute from August 13th 2016 through September 22nd 2016. Data weren't collected between September 9th and September 12th.

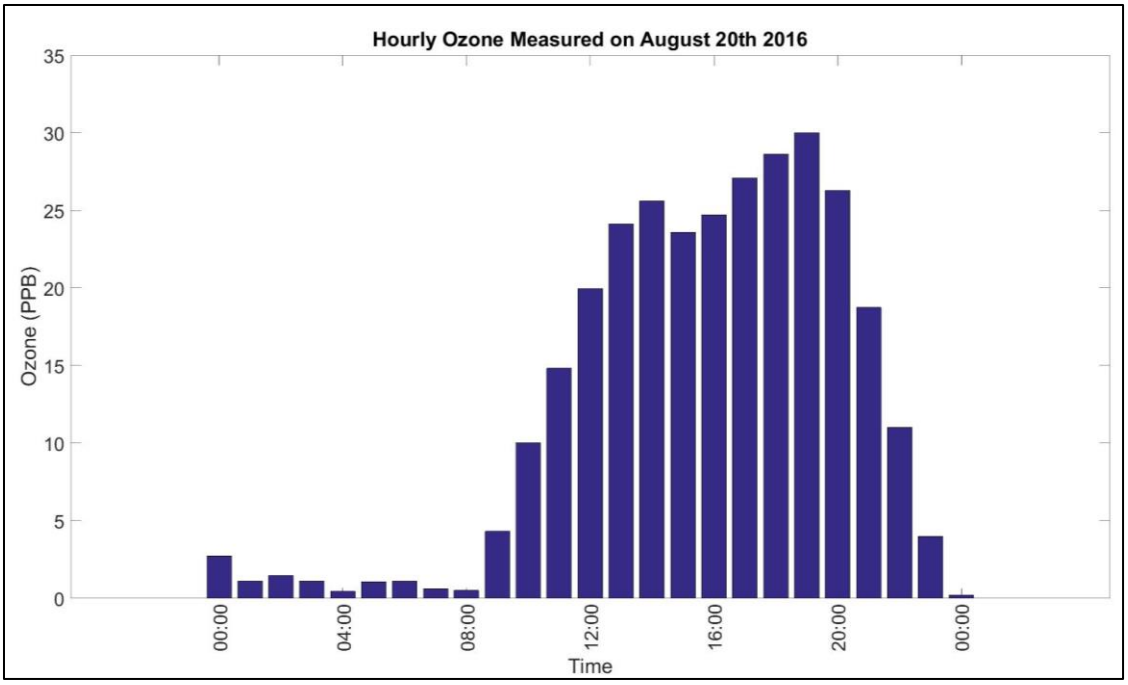

Figure 15. Hourly ozone measured on August 20th 2016.

Figure 15 shows the measured O_3 averaged every hour for August 20th 2016. The maximum levels typically occurred during the day and decreased after sunset. For August 20th and most other nights, the ozone levels are highest right after sunset and decrease to a minimum around sunrise. Figure 16 shows the hourly averaged O_3 between the hours of 19:00 CDT and 7:00 CDT for the full campaign. At night, the maximum O_3 observed was 53 ppb, while the minimum was 0.01 ppb.

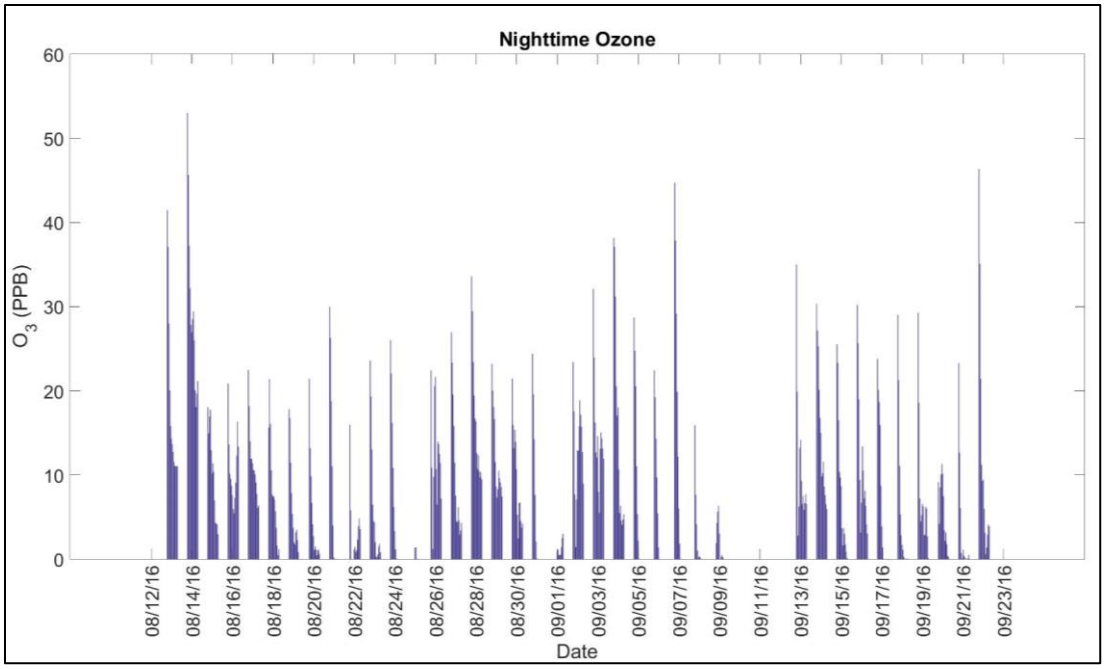

Figure 16. Hourly averaged ozone between the hours of 19:00 CDT and 7:00 CDT. Data weren't collected between September 9th and September 12th.

4.3.2. Nitric Oxide

Figure 17 shows the NO during the entire field campaign averaged every minute. Though spikes of up to 74 ppb occurred, the average NO was only 1.5 ppb. The maximum peaks occurred an hour or two after sunrise while the majority of the NO measurements hovered around 1 ppb.

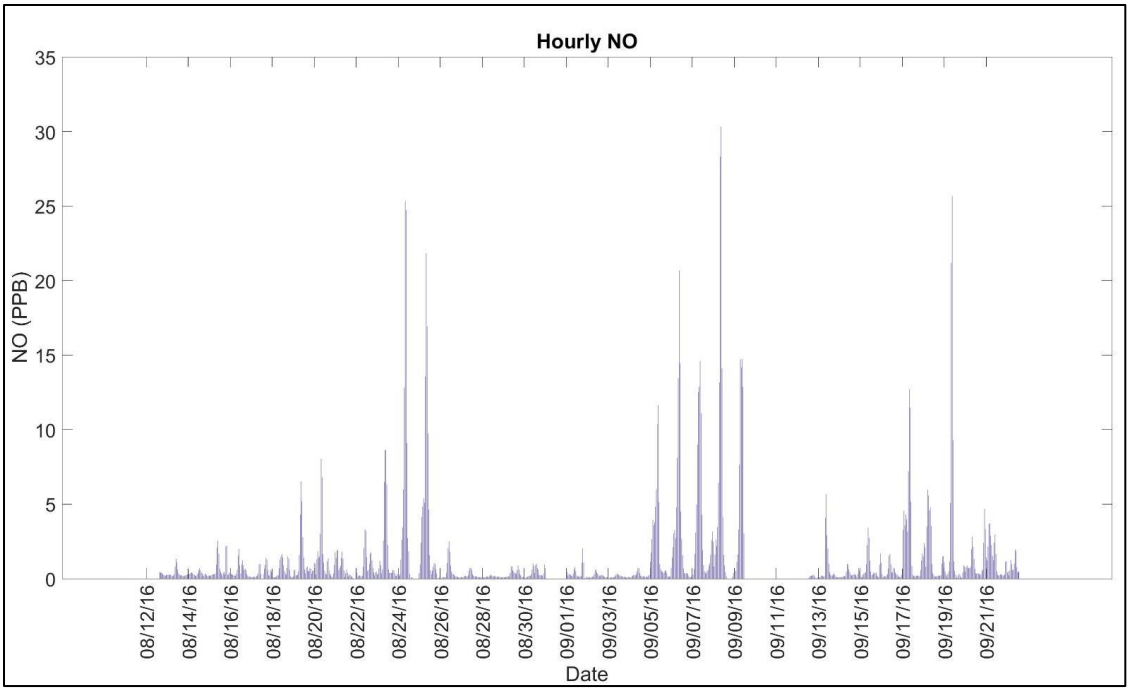

Figure 17. NO from August 13th 2016 through September 22nd 2016 averaged every minute. Data weren't collected between September 9th and September 12th.

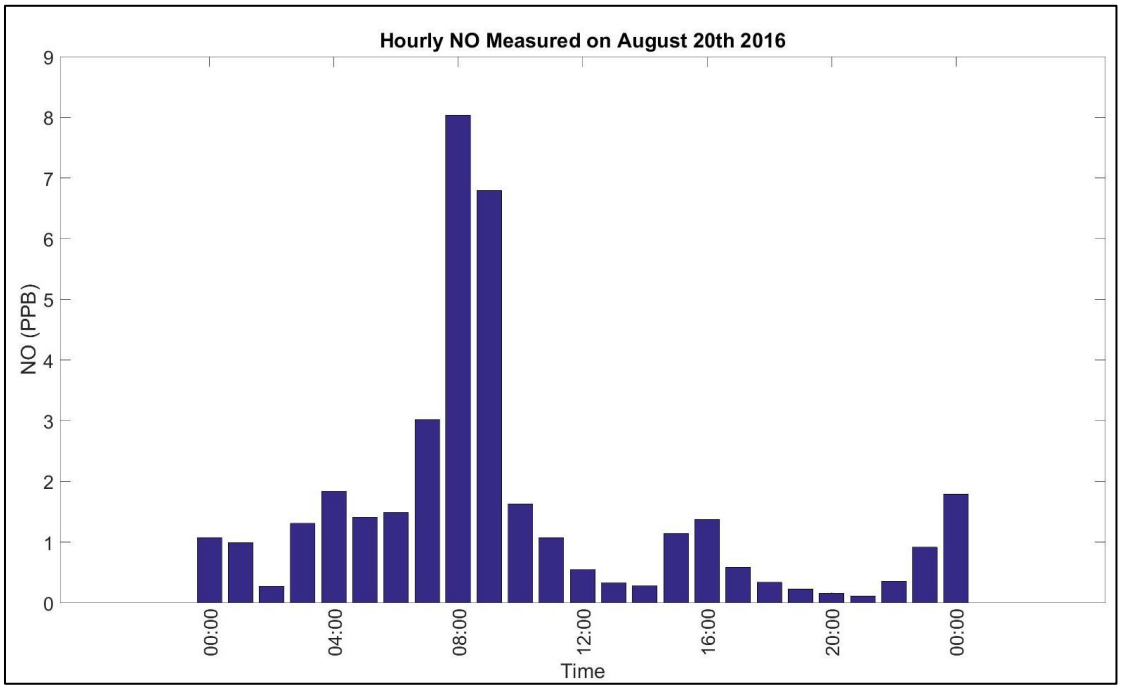

Figure 18. Hourly NO measured on August 20th 2016.

Figure 19 shows the hourly averaged NO between 19:00 CDT and 7:00 CDT. Unlike O_3, where the peak nighttime levels occurred directly after sunset, maximum NO measurements were very low after sunset and increased until sunrise. The maximum nighttime levels were only 14.7 ppb while the minimum was 0.01 ppb. The average nighttime NO was less than 1 ppb.

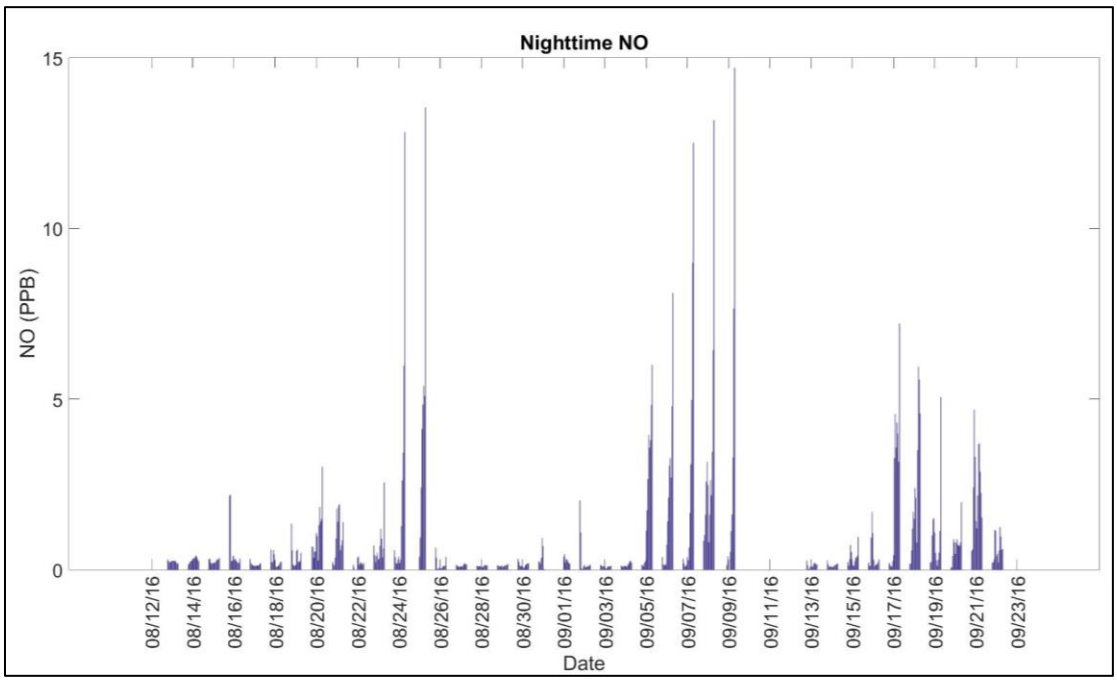

Figure 19. Hourly averaged NO between 19:00 CDT and 7:00 CDT. Data weren't collected between September 9th and September 12th.

4.3.3. Nitrogen Dioxide

Figure 20 shows NO_2 averaged every minute for the full campaign. Compared to NO, the peak measurements were lower only reaching 25 ppb. but the overall average

for the campaign is higher at 3.6 ppb. The minimum NO_2 levels occurred during the day, most likely driven by NO being created by the photolysis of NO_2.

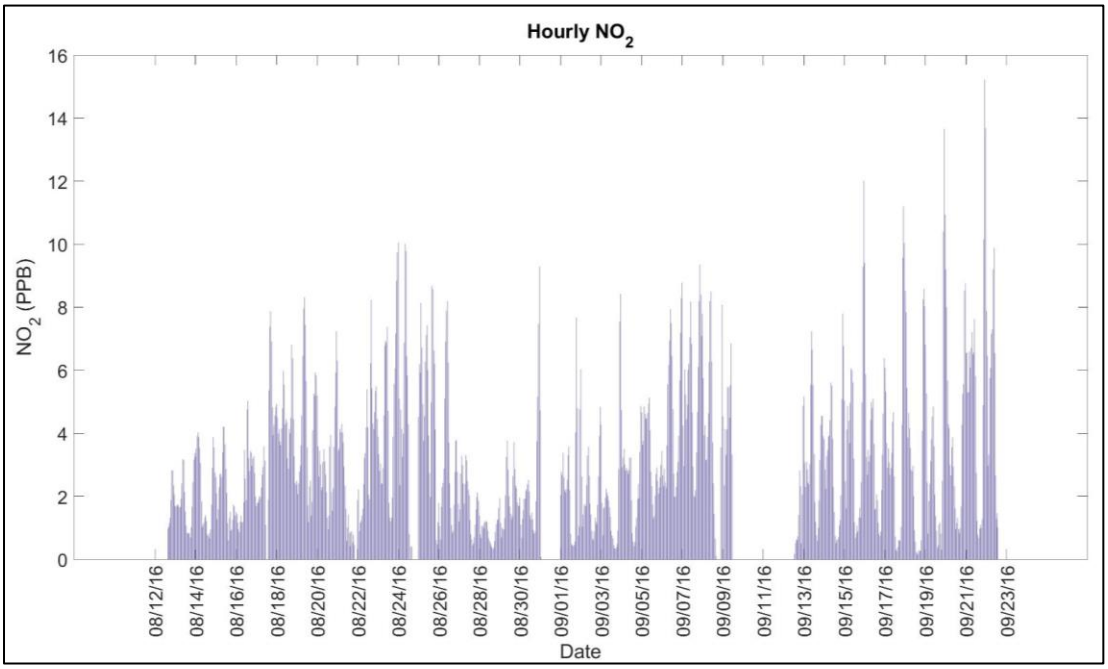

Figure 20. NO_2 averaged every minute. Data weren't collected between September 9th and September 12th.

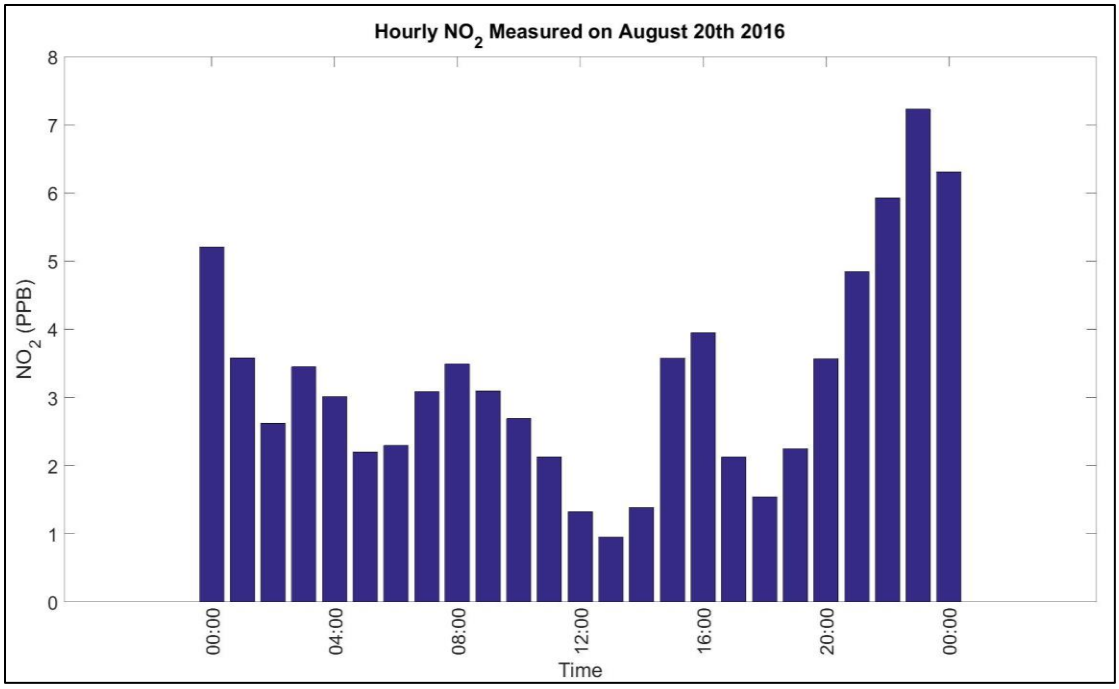

Figure 21. Hourly NO_2 measured on August 20th 2016

Figure 22 shows the hourly averaged NO_2 levels between 19:00 CDT and 7:00 CDT. At night, the maximum NO_2 measurements only reached 15 ppb, while the minimum was 0.07 ppb. The average nighttime NO_2 levels were similar to the full campaign at 3.25 ppb. Peaks observed at night were typically between sunset and midnight. Unlike O_3 where levels decreased at night, and NO where levels increased at night, NO_2 levels reached a peak and decreased to a steady state for the rest of the night.

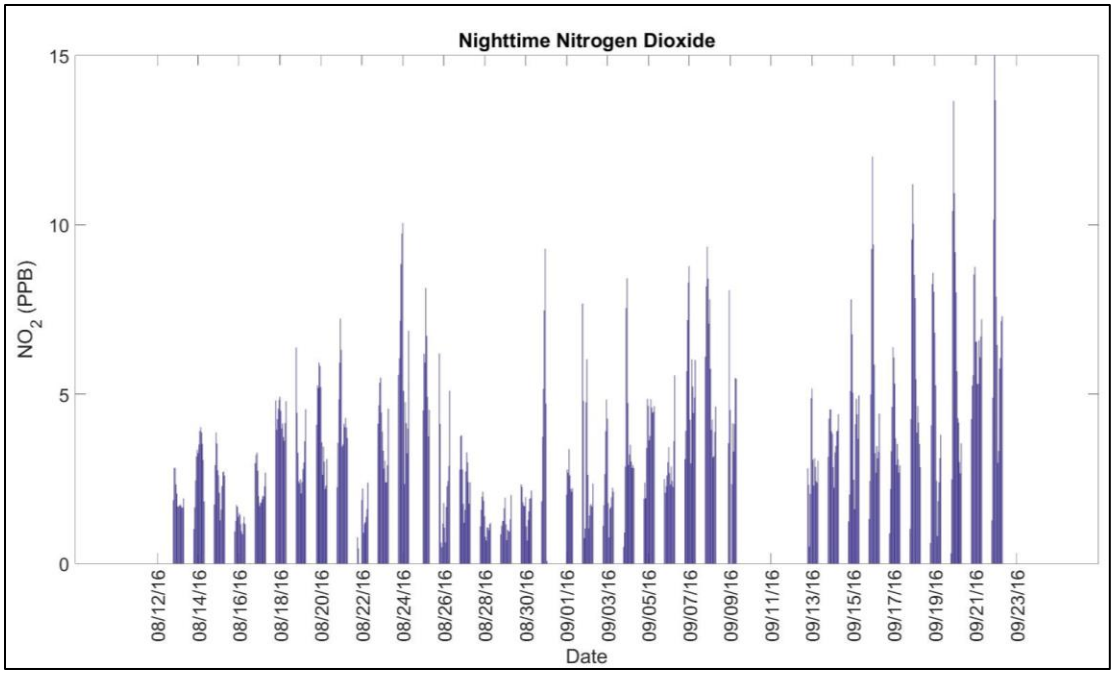

Figure 22. Hourly averaged NO_2 between 19:00 CDT and 7:00 CDT. Data weren't collected between September 9th and September 12th.

4.4. PTR-MS Data

PTR-MS data was also collected every minute. To calibrate the PTR-MS the compounds identified by the PTR-MS were mixed with zero air at ppb levels and the signal at the corresponding m/z signal was measured. The PTR-MS identified 21 compounds. Figures 23 - 26 shows the measurements of the compounds for the entire campaign while Table 3 shows m/z values and detection limits for each calibration species. The PTR-MS does not distinguish between different species at the same m/z signal. Camphene was the calibration species for the entire group of monoterpenes.

Fragmentation occurs within the PTR-MS, which can result in a response at smaller m/z values. These responses were not accounted for and species were only

measured at a single m/z value. The detection limits of the species were determined using Poisson statistics. Many species were near or below the detection limit for the entire campaign.

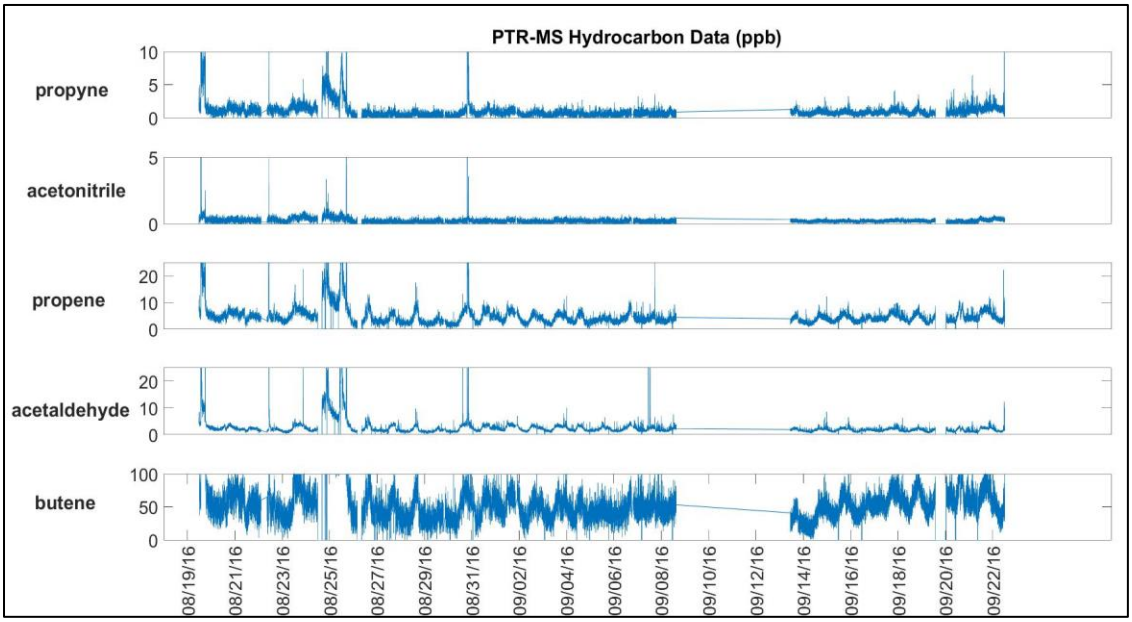

Figure 23. PTR-MS data for propyne, acetonitrile, propene, acetaldehyde, and butene. Data weren't collected between September 9th and September 12th.

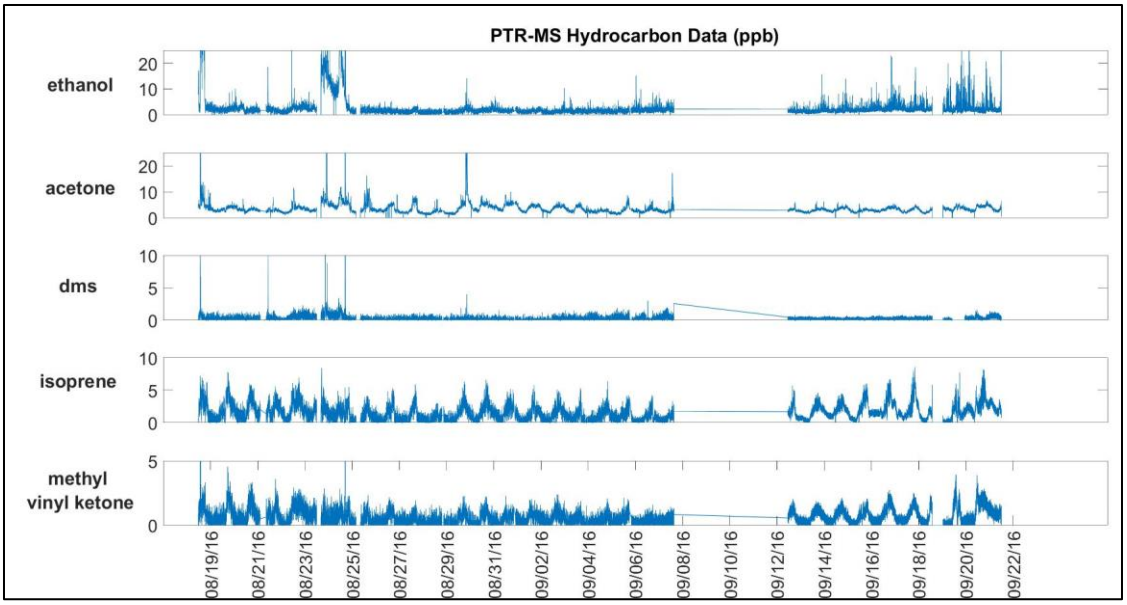

Figure 24. PTR-MS data for ethanol, acetone, dms, isoprene, and methyl vinyl ketone. Data weren't collected between September 9th and September 12th.

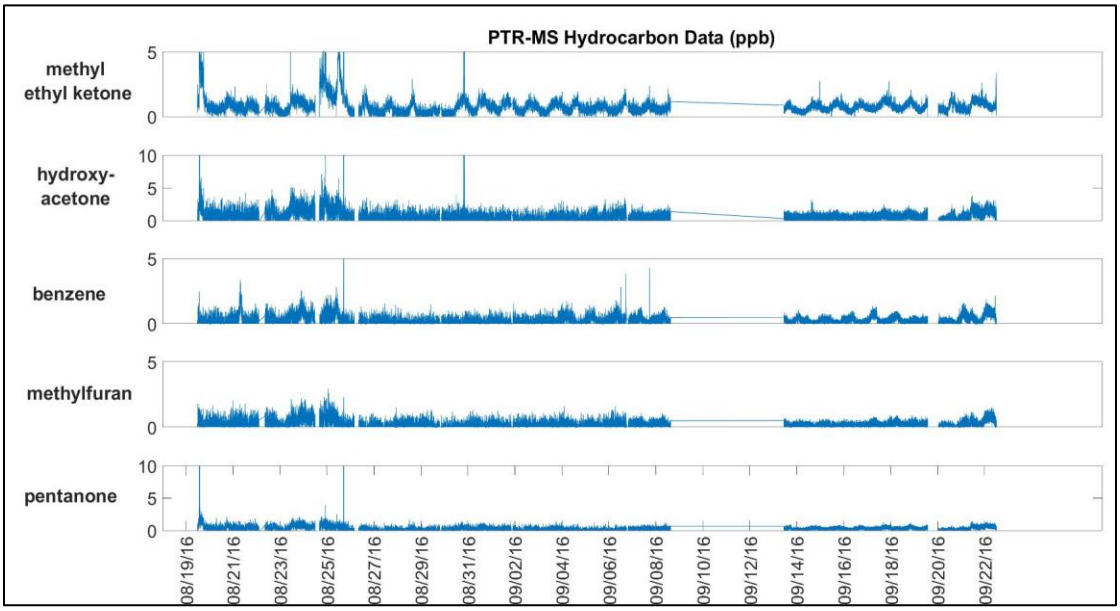

Figure 25. PTR-MS data for methyl ethyl ketone, hydroxyacetone, benzene, methylfuran, and pentanone. Data weren't collected between September 9th and September 12th.

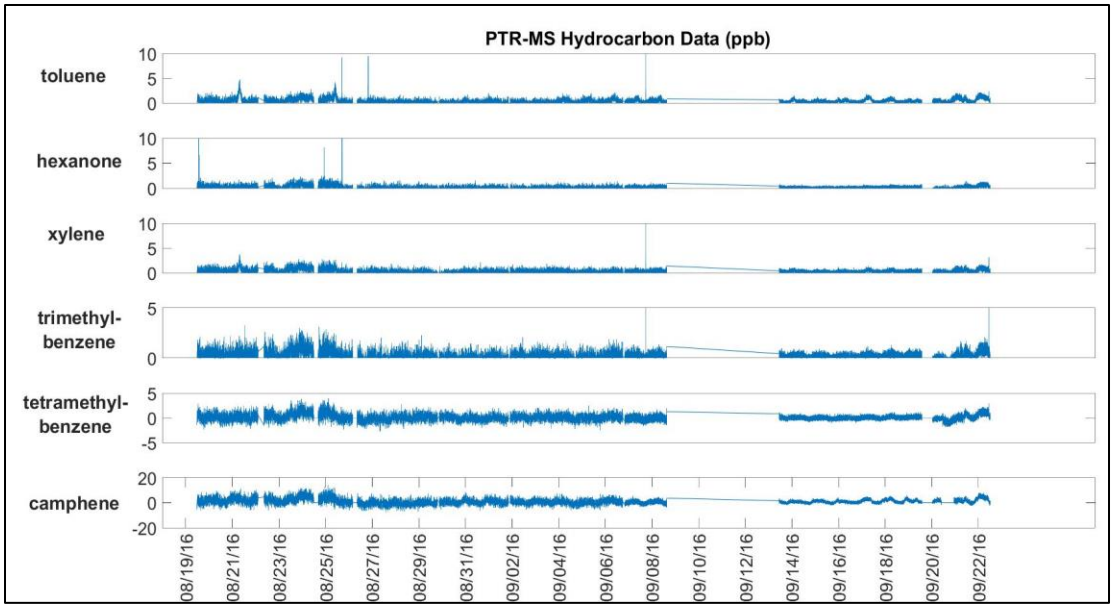

Figure 26. PTR-MS data for toluene, hexanone, xylene, trimethylbenzene, tetramethylbenzene, and camphene. Data weren't collected between September 9th and September 12th.

It will be shown later that the most important species with regards to nighttime NO_3· chemistry were at m69 and m137. These correspond with the calibration species of isoprene and camphene. For the rest of the data analysis, these two species will represent the biogenic volatile organic compounds that will be studied. The camphene species will encompass the entire monoterpene group. Due to high detection limits the monoterpene measurements had to be averaged over a 6 hour period to increase the accuracy.

Table 3. List of hydrocarbons from the PTR-MS including the m/z value used to identify the species and the detection limits.

Calibration Species	m/z value	Detection limit (ppbv)
Propyne	m41	1.0
Acetonitrile	m42	0.3
Propene	m43	1.4
Acetaldehyde	m45	0.4
Ethanol	m47	20
1-butane	m57	1.8
Acetone	m59	0.3
Dimethyl sulfide	m63	1.0
Isoprene	m69	1.5
Methyl vinyl ketone	m71	1.1
Methyl ethyl ketone	m73	0.6
Hydroxyacetone	m75	2.8
Benzene	m79	1.2
3-methylfuran	m83	1.0
3-pentanone	m87	1.1
Toluene	m93	1.2
3-hexanone	m101	1.5
m-xylene	m107	1.5
1,3,5-trimethylbenzene	m121	1.9
1,2,4,5-tetramethylbenzene	m135	2.5
Camphene	m137	4.0

Figure 27 shows the isoprene levels for the full field campaign. Measurements were averaged every minute until September 7th 2016 when averaging changed to every 30 seconds. Occasionally instrument drifts caused negative values but the occasional negative values did not affect the cyclical pattern of the data. The maximum isoprene level observed were 9 ppb while the average isoprene measurement was 1.6 ppb.

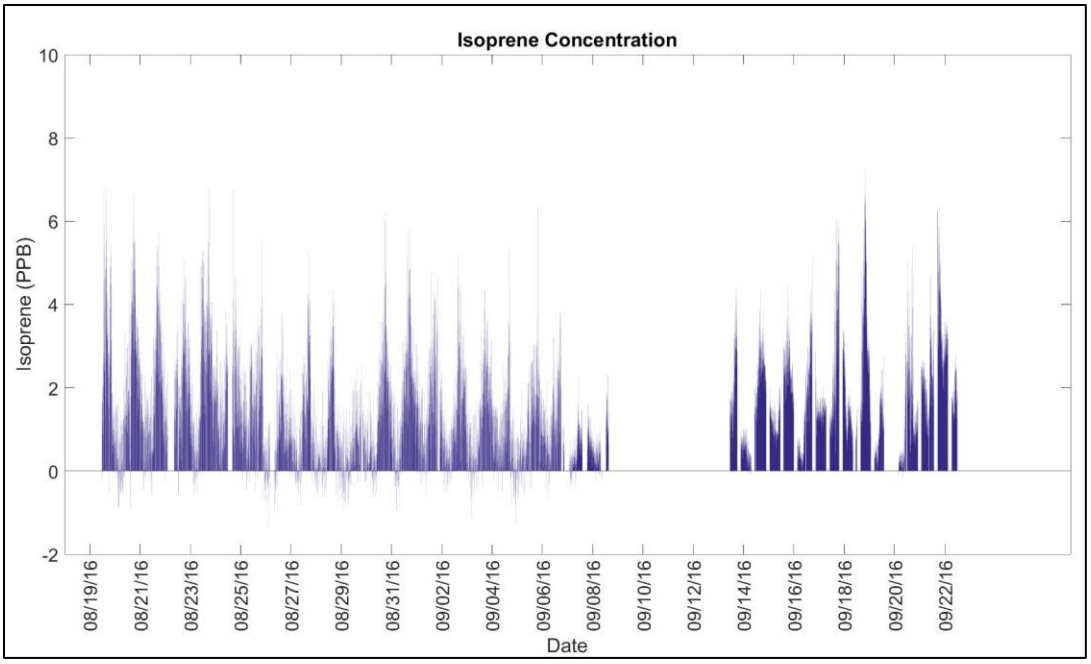

Figure 27. Isoprene averaged every 30 seconds to every minute. Data weren't collected between September 9th and September 12th.

Figure 28 shows the hourly averaged isoprene levels between 19:00 CDT and 7:00 CDT. Unlike the full isoprene data set, nighttime measurements were always greater than zero. At night, isoprene reached a maximum of 5.5 ppb and occasionally reached a minimum of zero. Peak measurements were typically observed directly at sunset and slowly decreased to lower values near sunrise. The average isoprene level during the night was 1.24 ppb.

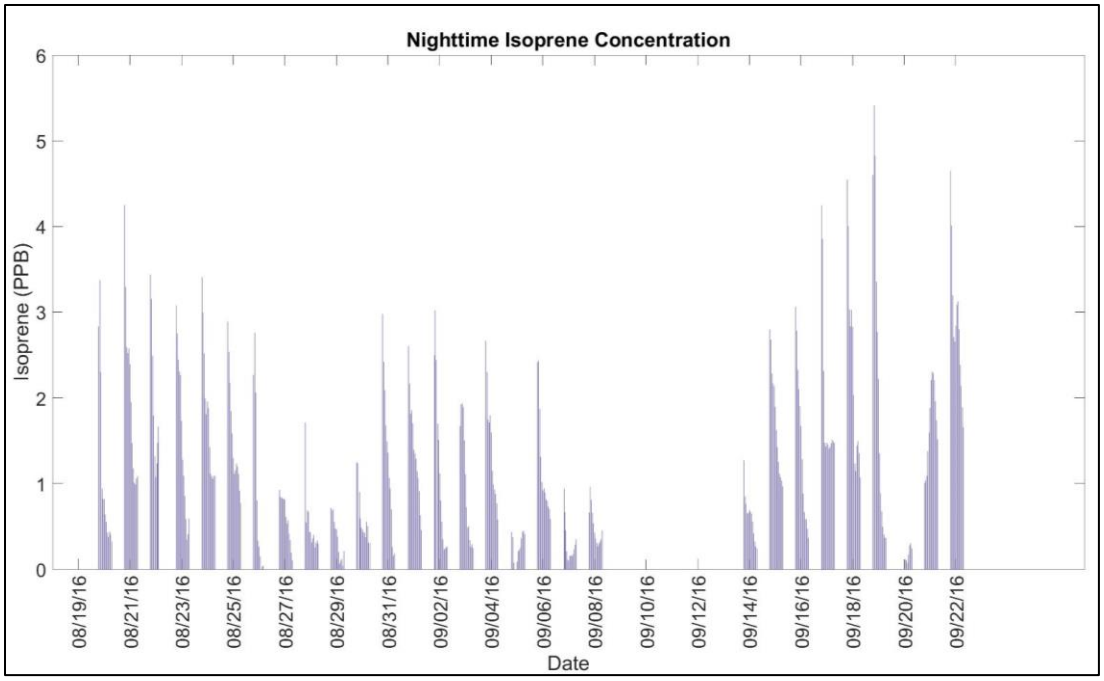

Figure 28. Hourly averaged isoprene between 19:00 CDT and 7:00 CDT. Data weren't collected between September 9th and September 12th.

The m137 signal corresponds to the monoterpenes. Figure 29 shows the hourly averaged monoterpene measurements for the full field campaign. Due to high detection limits and drifts in the instrument, the hourly data is not extremely reliable and contains many negative values. To remedy this, 12 hour averages were calculated and if the average was negative then the entire data for that time period was shifted upwards until the average was zero. To combat the detection limit problem the data was averaged every 6 hours. This data is shown in Figure 30. This allowed for more reliable data, but also lost some of the cyclical pattern that typically would be observed over shorter time frames.

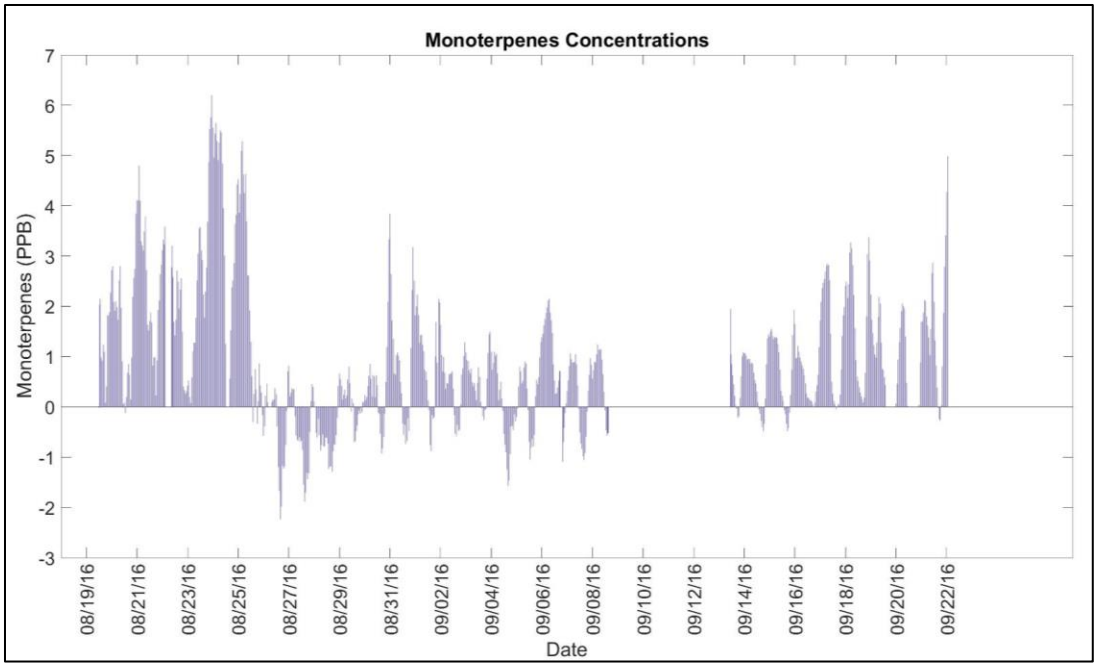

Figure 29. Monoterpenes averaged every minute between August 19th 2016 and September 23rd 2016. Data weren't collected between September 9th and September 12th.

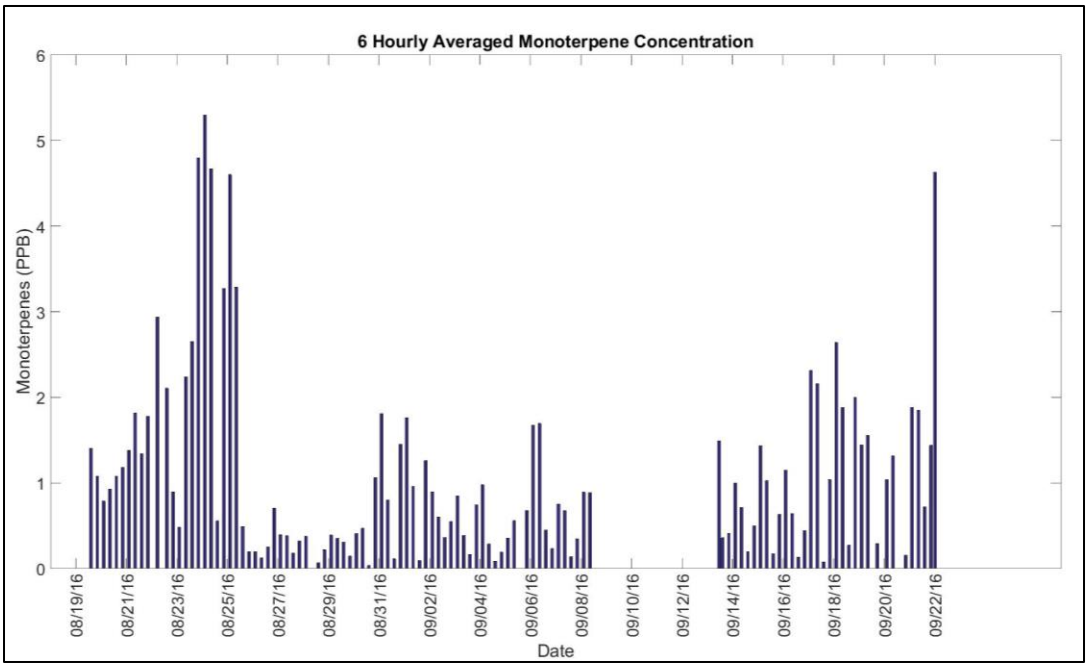

Figure 30. Monoterpenes averaged every six hours. Data weren't collected between September 9th and September 12th.

Within the 6 hour averages the peaks were typically between 6:00 CDT and 12:00 CDT. Once the instrumentation shift was accounted for, the maximum 6 hour average was 5.3 ppb and the average for all of the data was 1.05 ppb. Next, the nighttime monoterpene six hour averages were separated, shown in Figure 31.

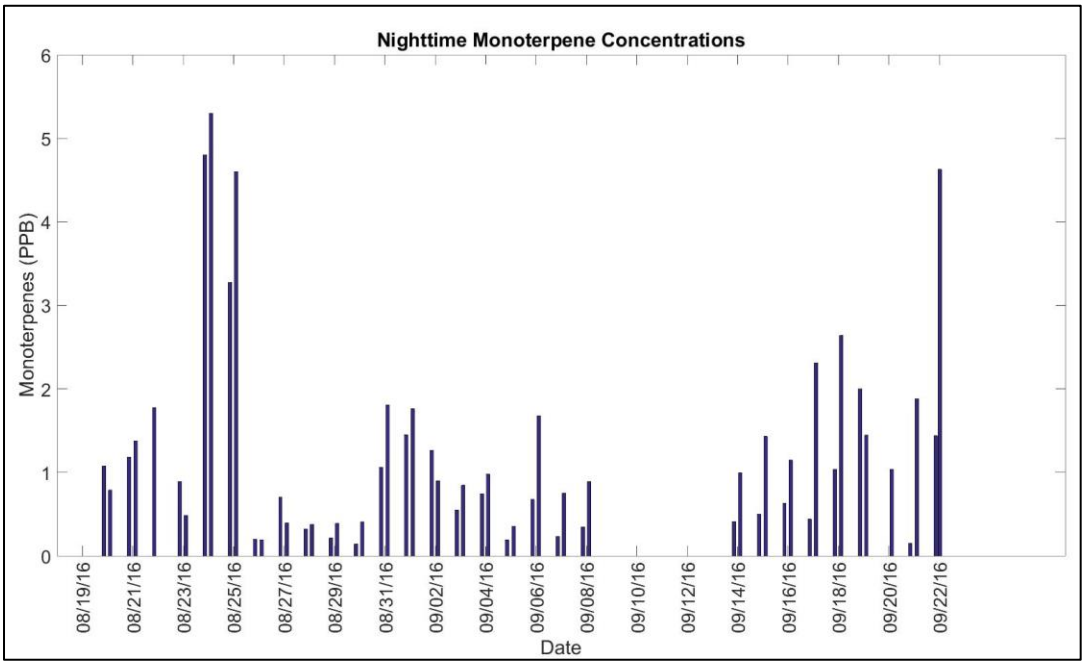

Figure 31. Monoterpenes averaged every 6 hours between 19:00 CDT and 7:00 CDT. Data weren't collected between September 9th and September 12th.

4.5. NO_3· Estimate

To estimate the levels of NO_3·, an equilibrium expression was determined using relevant reactions and reaction rates adapted from Brown et al. (2013). These reactions and reaction rates are shown in Table 4.

Table 4. Reactions and reaction rates used to develop a NO_3· equilibrium equation.

Reactions	Reaction Rates
$NO_2 + O_3 \rightarrow NO_3\cdot + O_2$	$1.4 \times 10^{-13} \exp(-2470/T)$
$NO_2 + NO_3\cdot + M \rightarrow N_2O_5 + M$	$1.9 \times 10^{-12} (T/300)^{0.2}$
$NO_3\cdot + NO \rightarrow NO_2$	$1.8 \times 10^{-11} \exp(110/T)$

To create this equilibrium equation the production and destruction of NO_3· are set equal to each other and NO_3· levels are determined:

k_1 $NO_2 + O_3 \rightarrow NO_3\cdot + O_2$ (8)

k_2 $NO_2 + NO_3\cdot + M \rightarrow N_2O_5 + M$ (9)

k_3 $NO_3\cdot + NO \rightarrow NO_2$ (10)

$$k_1[NO_2][O_3] = k_2[NO_2][NO_3] + k_3[NO][NO_3\cdot] \quad (11)$$

$$k_1[NO_2][O_3] = [NO_3\cdot](k_2[NO_2] + k_3[NO]) \quad (12)$$

$$\frac{k_1[NO_2][O_3]}{k_2[NO_2]+k_3[NO]} = [NO_3\cdot] \quad (13)$$

Once the equilibrium equation was established, the measurements from the trace gas analyzers were used. Figure 32 shows estimated NO_3· for the full field campaign without any hydrocarbon reactions or any daytime photolysis being accounted for.

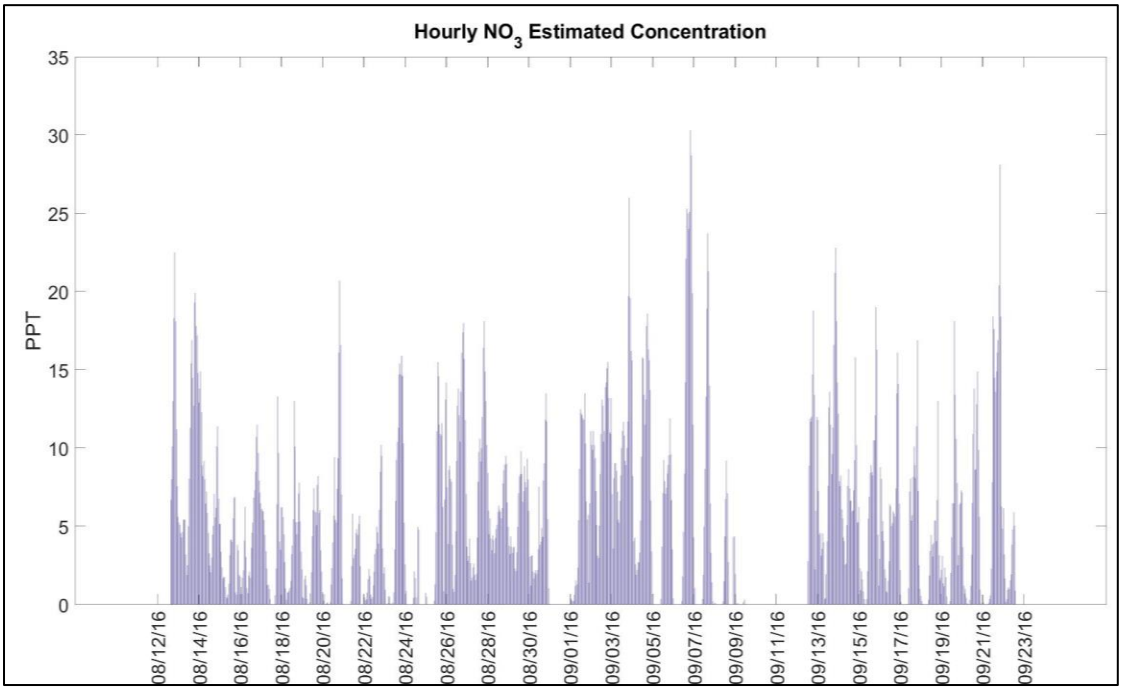

Figure 32. Hourly NO_3· concentrations estimated using the developed equilibrium equation. Data weren't collected between September 9th and September 12th.

Once the NO_3· concentration was found, the hydrocarbons were introduced individually to the destruction side of the equilibrium equation. New NO_3· concentrations were estimated that now include the impact of the individual hydrocarbons. Most of the hydrocarbons had no effect on NO_3·, so only isoprene and monoterpene reactions will be included in determining the new nitrate radical estimated concentrations.

Figure 33 shows estimated NO_3· including isoprene reactions. The reaction rate used for reactions between nitrate radical and isoprene was 7 x 10^{-13} cm^3 $molecule^{-1}$ s^{-1} (Brown and Stutz, 2012). Figure 34 shows the difference between estimated NO_3· without any hydrocarbons and estimated NO_3· including isoprene reactions.

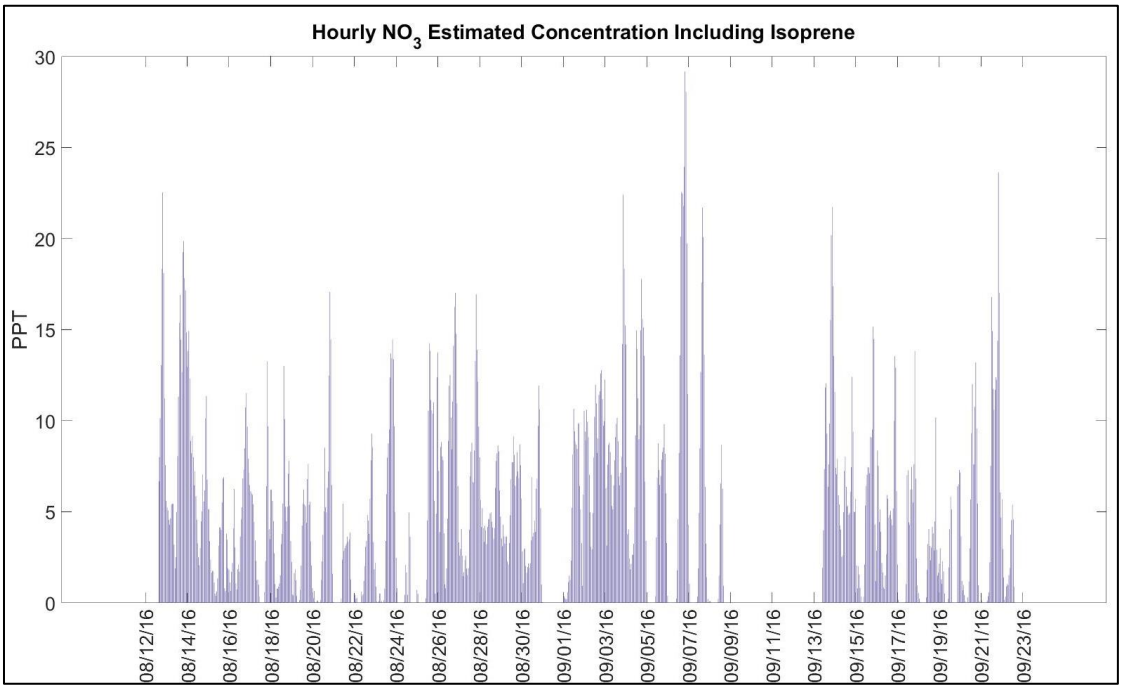

Figure 33. Hourly NO_3· estimated with isoprene reactions added to the equilibrium equation. Data weren't collected between September 9th and September 12th.

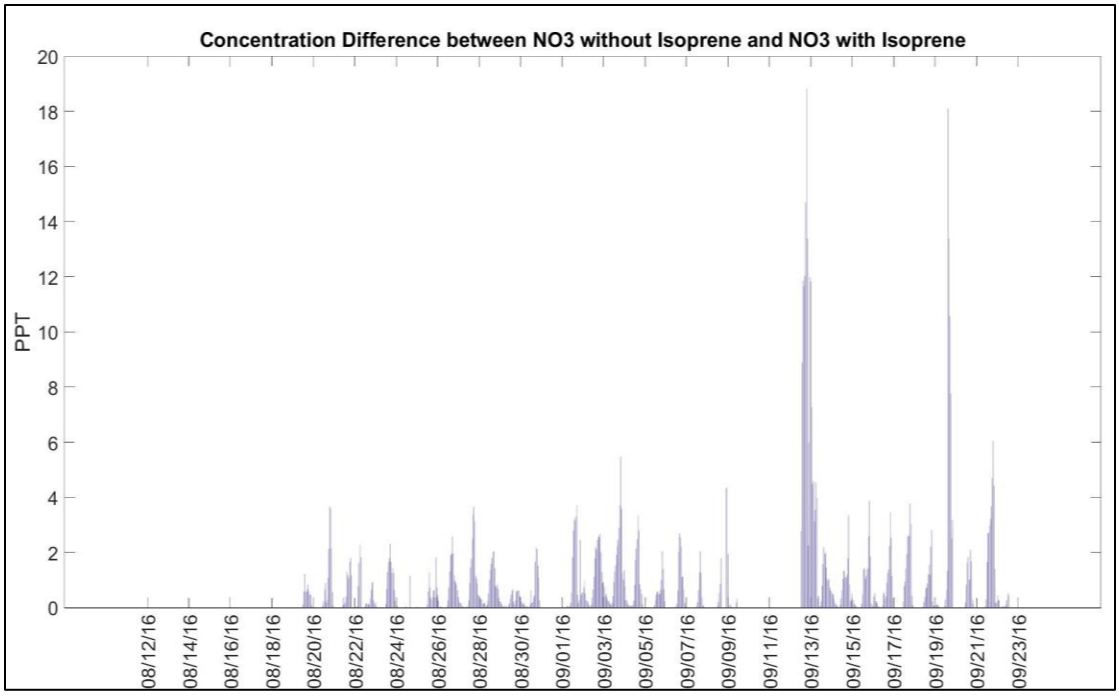

Figure 34. Difference between the NO_3· without including hydrocarbons and the NO_3· including isoprene reactions. Data weren't collected between September 9th and September 12th.

Figure 35 shows the estimated NO_3· averaged over every six hours both without hydrocarbons and with reactions with monoterpenes. The reaction rate used for the reaction between NO_3· and monoterpenes was 4.34×10^{-12} cm^3 $molecule^{-1}$ s^{-1} (Brown and Stutz, 2012). This reaction rate was determined by assuming that the amount of α-pinene and β-pinene making up the monoterpenes was exactly 50/50. Figure 36 shows the difference in concentration between these two estimates. Except for a few spikes in the data, the typical difference was under 4 ppt,

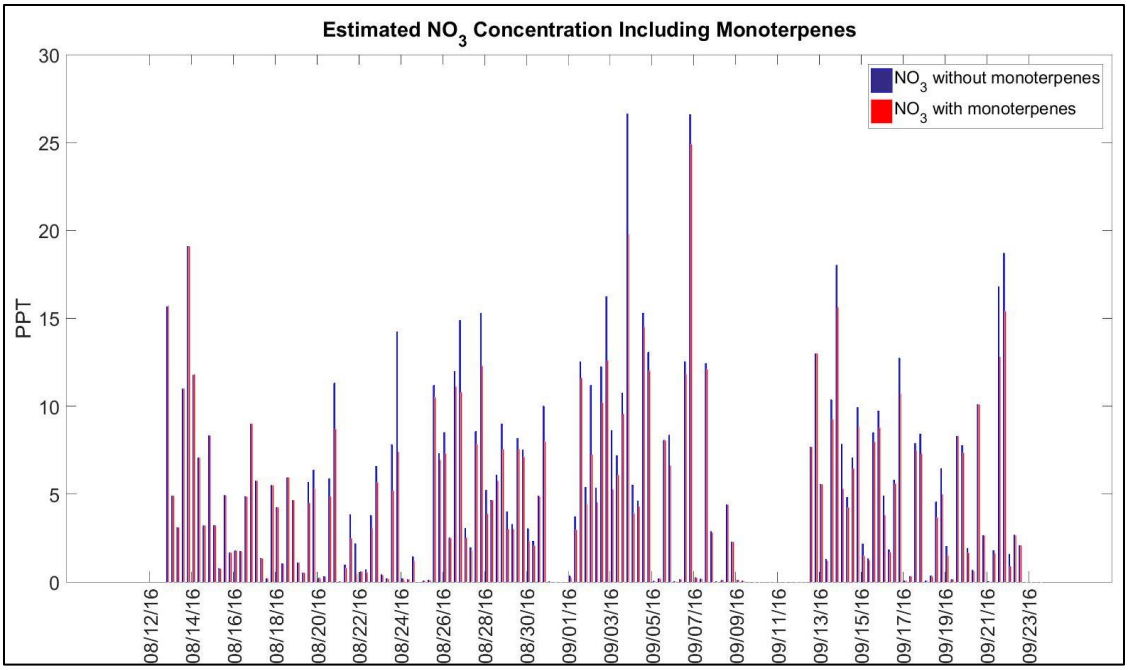

Figure 35. Estimated NO_3· without monoterpenes (red) and with reactions with monoterpenes (blue). Data weren't collected between September 9th and September 12th.

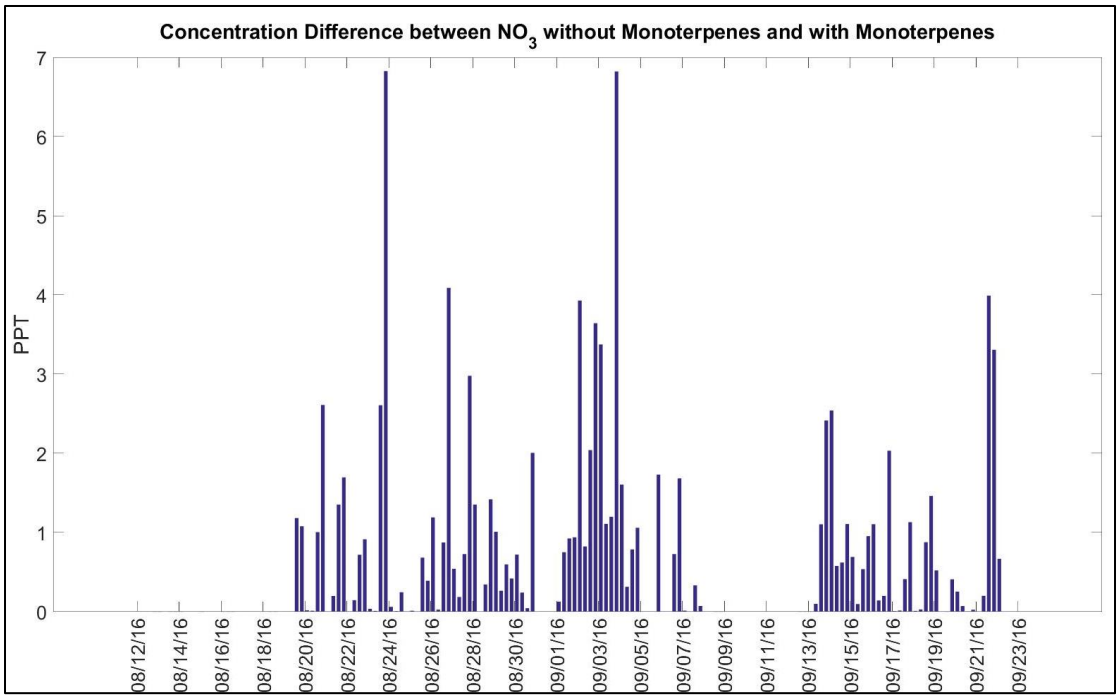

Figure 36. Difference between NO_3· without monoterpenes and with reactions with monoterpenes. Data weren't collected between September 9th and September 12th.

Nighttime NO_3· including these hydrocarbons were then calculated. Figure 37 shows these estimations. NO_3· including isoprene reactions were averaged every hour, but the calculations including the reactions with the monoterpenes were averaged every six hours. The 6 hour long averages made it difficult to determine a definitive pattern of nighttime nitrate radical. The estimated NO_3· with isoprene reactions were always higher than those including only the monoterpenes reactions. Thus, at night the monoterpenes are reacting more with NO_3·. For almost every night, the estimated levels were higher between sunset and midnight than midnight and sunrise. The only nights where the levels were smaller after sunset compared to levels measured between midnight and sunrise were on August 26th, and September 2nd.

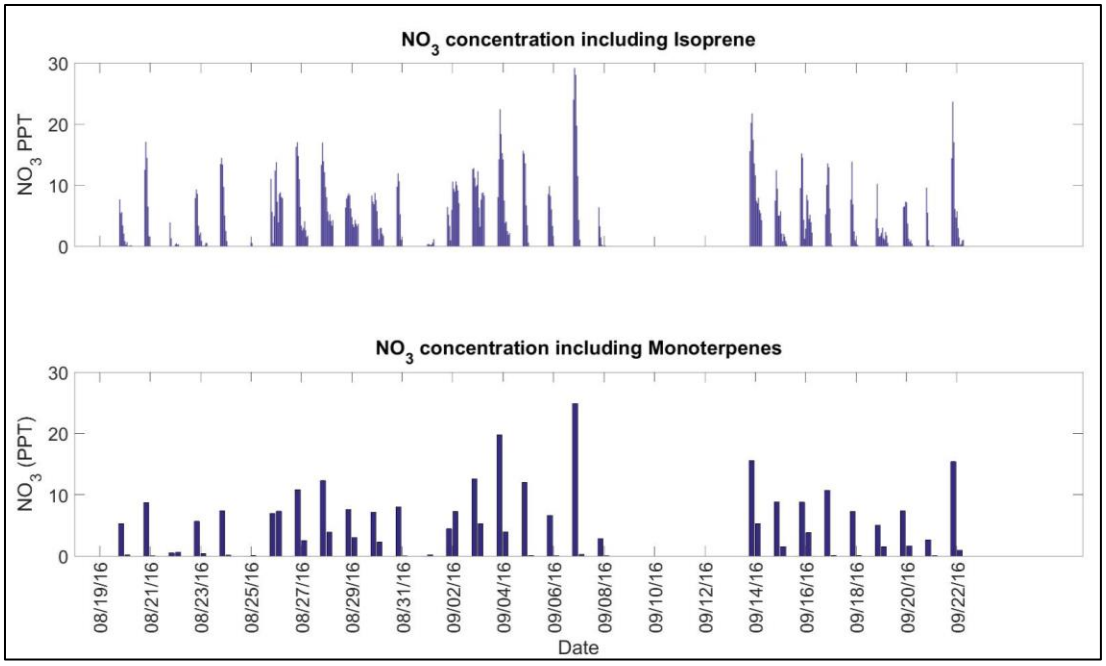

Figure 37. Nighttime NO_3· concentrations including only isoprene (top) and only monoterpenes (bottom). Concentrations were averaged every hour for those including isoprene and averaged every six hours for concentrations including monoterpenes. Data weren't collected between September 9th and September 12th.

Both isoprene and the monoterpenes serve as a sink for NO_3·, thus both oxidation reactions must be included to estimate NO_3·. Figure 38 shows estimated NO_3· including both isoprene and the monoterpenes reactions between 19:00 CDT and 7:00 CDT averaged every six hours.

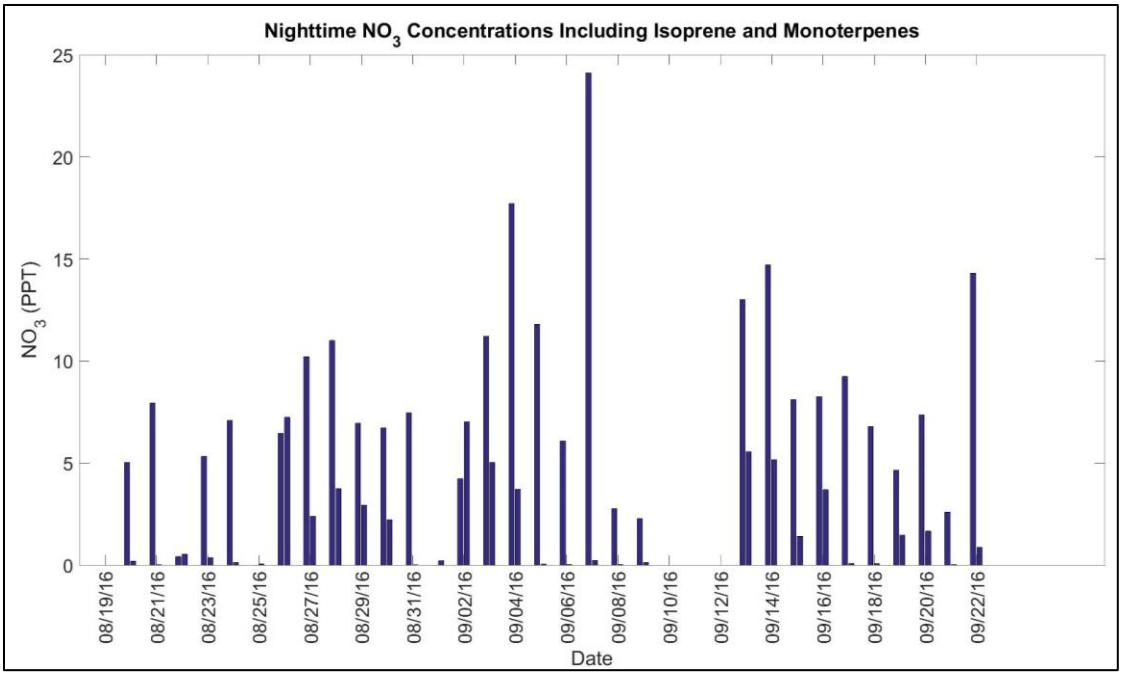

Figure 38. Estimated NO_3· including all hydrocarbons between 19:00 CDT and 7:00 CDT. Data weren't collected between September 9th and September 12th.

4.6. SOA Estimate

Once the nitrate radical was estimated, the estimated SOA levels could be calculated:

$$k_{isoprene}[NO_3][Isoprene] \quad (14)$$

$$k_{monoterpenes}[NO_3][Monoterpenes] \quad (15)$$

After this was done, the percent yield was used to determine the SOA contributed by each hydrocarbon. These yields were adapted from Ng et al., (2008, 2017) and were 4% for α-pinene, 44% for β-pinene, and 15% for isoprene. The SOA yield was then

converted to micrograms per cubic meter using the molecular weights of the various hydrocarbons. Due to $NO_3\cdot$ only being an important oxidant after sunset, only the SOA production between sunset and sunrise was calculated. Figure 39 shows these calculated levels.

These SOA yields show that reactions with β-pinene produces SOA an order of magnitude higher than both α-pinene oxidation and isoprene oxidation. SOA formed through isoprene oxidation was typically higher than SOA formed through α-pinene oxidation.

A large spike in the SOA formed through the monoterpenes reactions was observed on the evening of August 23rd. Both the monoterpenes and $NO_3\cdot$ were not at a maximum, but were both high enough that SOA formation was maximum. These optimal conditions were only observed on this particular evening.

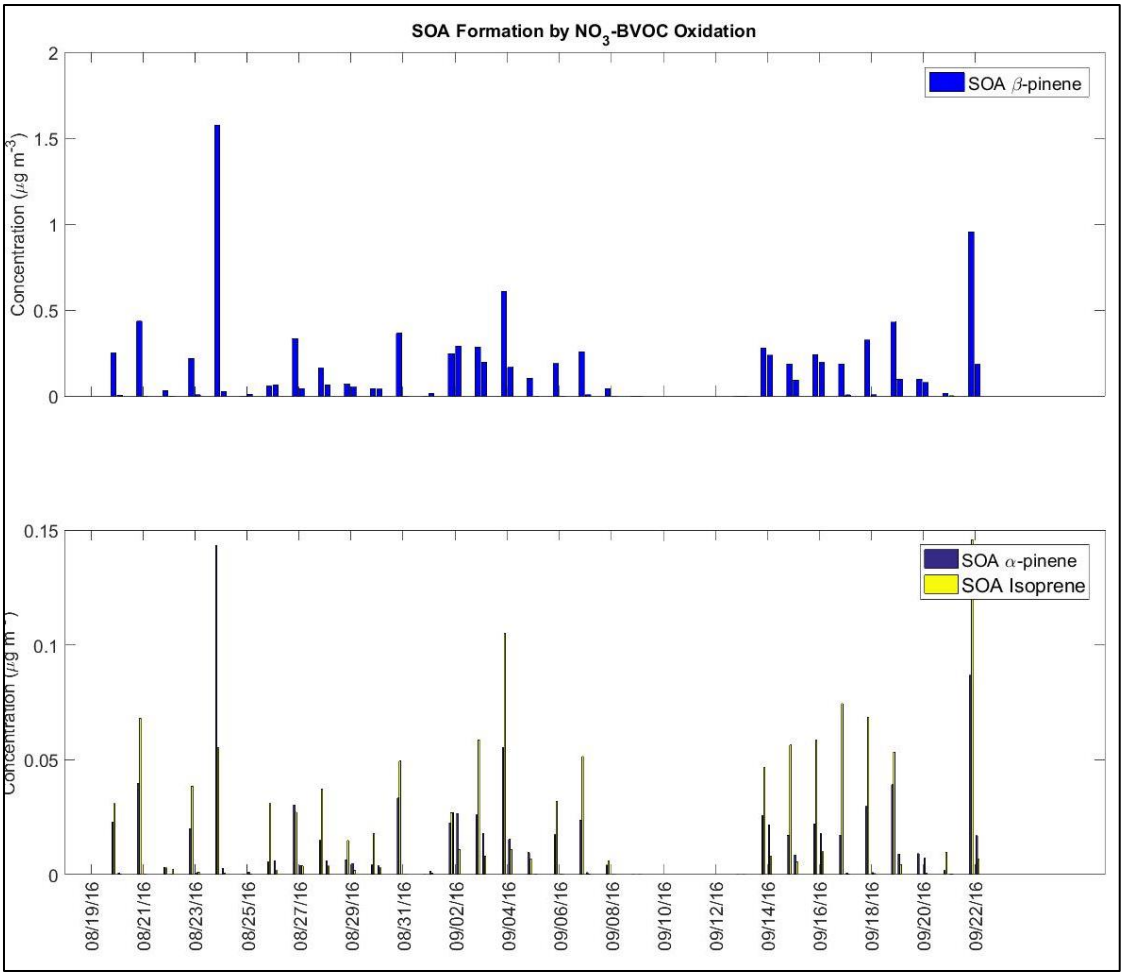

Figure 39. SOA formation through NO_3· reactions with β-pinene (top), α-pinene (bottom, purple), and isoprene (bottom, yellow). Data weren't collected between September 9th and September 12th.

The estimated SOA formation was based on the calculated NO_3· levels using trace gas analyzer data and hydrocarbon data from the PTR-MS. These measurements were all collected from ambient air at the field site, but to be certain that this formation is actually happening there needs to be similar growth happening inside of the chamber. The trace gas analyzers only sampled from inside of the chamber for a few days, but these measurements did show that typically the measurements observed in surrounding

ambient air were also observed inside of the chambers. To confirm the estimated SOA formation, the chamber growth rate was averaged every six hours for the corresponding days.

Due to SOA formation being highest from β-pinene oxidation, it would seem likely that growth rates observed inside the chamber would similarly match the SOA formation estimates from the oxidation of monoterpenes. This comparison is shown in Figure 40 for β-pinene and Figure 41 for α-pinene. Due to the monoterpenes being measured as one group, the main difference between the SOA formed through β-pinene and α-pinene is their percent yields. Therefore, the SOA graphs will be the same except for their magnitude. The SOA formation, in $\mu g\ m^{-3}$, and the growth rate, in $nm\ hr^{-1}$, have some similarities but there are multiple instances where growth is seen in the chamber but estimations show low SOA. From August 25th through August 31st there is a lot of growth observed inside the chamber, but estimated SOA formation from the oxidation of the monoterpenes is quite low. The growth rates could be caused by the oxidation of another species besides the monoterpenes. On the evening of August 23rd 2016 between sunset and midnight the estimated SOA formation from the oxidation of monoterpenes is at a maximum but the actual growth rate observed inside the chamber was very low. There was still some growth seen during that time, but it is far lower than estimated. During this specific evening, the relative humidity was at or near 100% between sunset and midnight. With high relative humidity, the following reaction proceeds more rapidly:

$$N_2O_5 + H_2O \rightarrow 2HNO_3 \qquad (16)$$

This reaction could result in a high NO_3· bias during times of high relative humidity. The reaction cycle of N_2O_5 in the creation and destruction of NO_3· was not included in the NO_3· equilibrium equation used to estimate NO_3·.

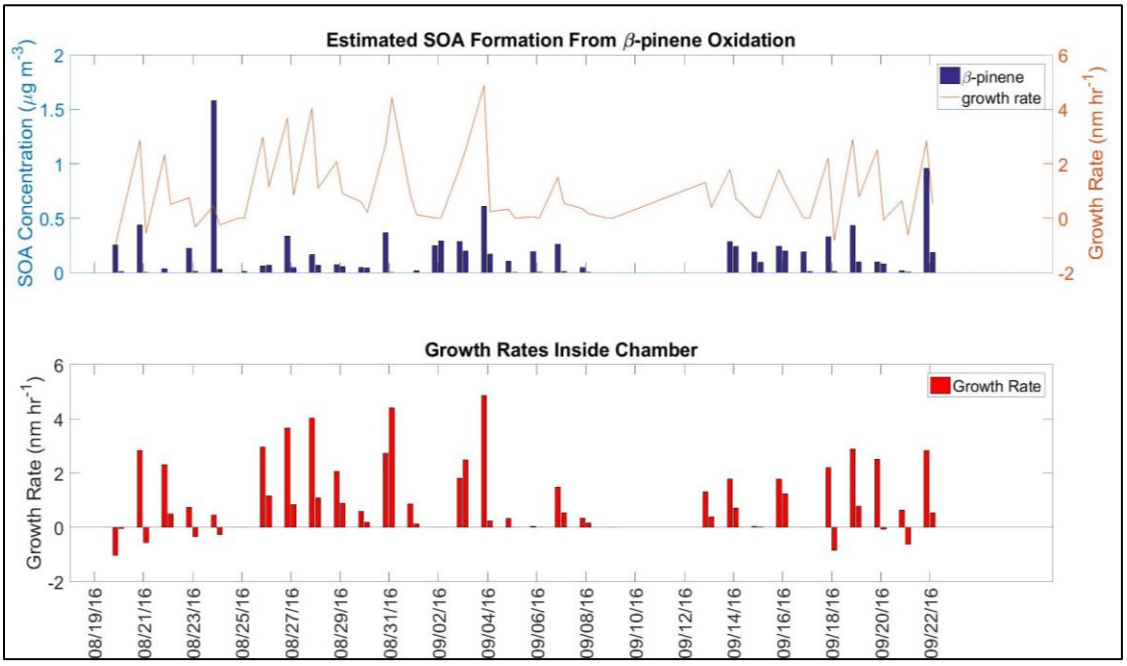

Figure 40. Comparison of SOA formation from β-pinene oxidation (top) and observed chamber growth rates (bottom). Data weren't collected between September 9th and September 12th.

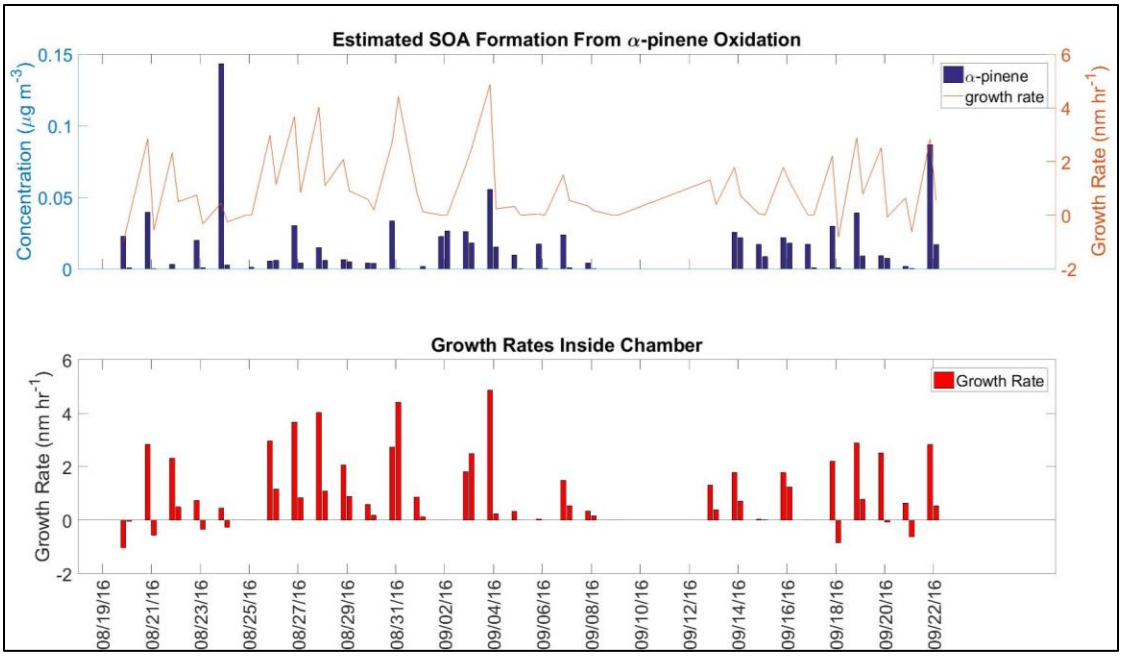

Figure 41. Comparison of SOA formation from α-pinene oxidation (top) and observed chamber growth rates (bottom). Data weren't collected between September 9th and September 12th.

The comparison of estimated SOA formation from isoprene oxidation and observed chamber growth rates is shown in Figure 42. Like the comparison with the SOA formation from monoterpenes oxidation, the SOA formation from isoprene oxidation and the growth rates inside the chamber are very similar. During the campaign while all instruments were measuring, the growth rate pattern is very similar to the estimated SOA formation. The only days of significant differences are August 19th, August 24th, August 31st, and September 22nd. The over estimation of SOA on the 24th can be explained by the N_2O_5 destruction discussed earlier. On August 31st, the estimated NO_3· for that time period is very small, but according to the growth rates

observed in the chamber there must be SOA formation occurring. This could possibly be due to the neglecting of N_2O_5 in the estimation of NO_3·.

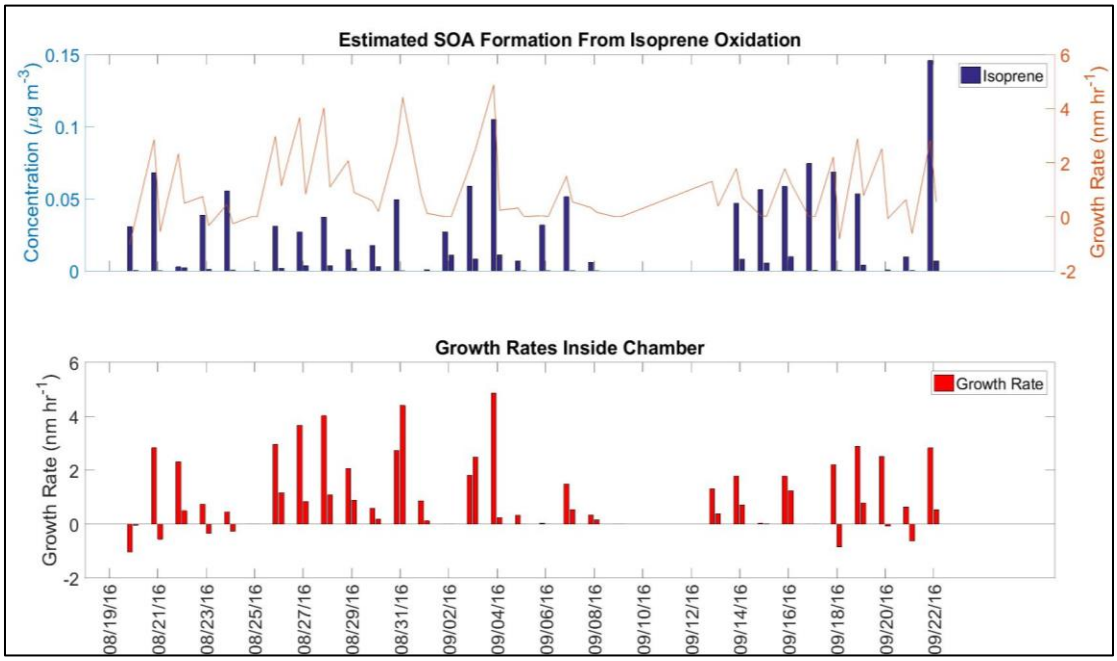

Figure 42. Comparison of SOA formation from isoprene oxidation (top) and observed chamber growth rates (bottom). Data weren't collected between September 9th and September 12th.

Visual comparison of SOA formation from the oxidation of BVOCs and chamber growth rate does not provide the most accurate interpretations. Statistical analysis was done on the data to determine any correlation between estimated SOA formation and growth rate. The first method was done using the Pearson method. This is a measure of the linear correlation between two variables. This is shown in Table 5.

Table 5. Correlation Coefficient from Pearson method comparing SOA formation from BVOC oxidation and growth rate.

	SOA α-pinene	SOA β-pinene	SOA isoprene	Growth Rate
SOA α-pinene	1.00	9.99×10^{-1}	7.20×10^{-1}	3.31×10^{-1}
SOA β-pinene	9.99×10^{-1}	1.00	7.18×10^{-1}	3.33×10^{-1}
SOA isoprene	7.20×10^{-1}	7.18×10^{-1}	1.00	5.03×10^{-1}
Growth Rate	3.31×10^{-1}	3.33×10^{-1}	5.03×10^{-1}	1.00

The correlation coefficient between growth rate and estimated SOA formation from the oxidation of monoterpenes is near 0.33 while the coefficient between growth rate and estimated SOA formation from the oxidation of isoprene is 0.50. A correlation coefficient close to 1 is a perfect correlation, while a coefficient of zero is no correlation. These numbers show that there is some correlation between growth and estimated SOA formation from BVOC oxidation, but the correlation with isoprene caused SOA is higher than that of the monoterpenes. A p-test was conducted to determine if the calculated correlation coefficients are significant. Using an α-value of 0.05, the p-values for all three correlation coefficients were greatly below 0.05. This shows that the Pearson method correlation coefficients may be small, but they are significant.

Table 6. Correlation Coefficient from Spearman method comparing SOA formation form BVOC oxidation and growth rate.

	SOA α-pinene	SOA β-pinene	SOA isoprene	Growth Rate
SOA α-pinene	1.00	1.00	8.90×10^{-1}	4.55×10^{-1}
SOA β-pinene	1.00	1.00	8.90×10^{-1}	4.55×10^{-1}
SOA isoprene	8.90×10^{-1}	8.90×10^{-1}	1.00	4.43×10^{-1}
Growth Rate	4.55×10^{-1}	4.55×10^{-1}	4.43×10^{-1}	1.00

Next, the Spearman's rank correlation coefficient was determined for these variables. This method of analysis assesses the linearity of monotonic relationships. It is a nonparametric measure of rank correlation. These correlation coefficients are shown in Table 6. Unlike the Pearson method, these coefficients do not show a higher correlation with isoprene. Instead, the correlation coefficients for both hydrocarbons are around 0.45. A perfect Spearman correlation of 1 occurs when each of the variables is a perfect monotone function of the other. A coefficient of 0.45 is not perfect but it shows that there is some correlation between growth rate and estimated SOA formation. A p-test was also conducted for the Spearman method correlation coefficients. An α-value of 0.05 was also used for this test. Again, for all three correlation coefficients, the calculated p-values were much smaller than 0.05. Thus, the Spearman method correlation coefficients are also significant even if they are low correlation coefficients.

5. SUMMARY AND CONCLUSIONS

5.1. Summary

The reactions between nighttime nitrate radical and biogenic volatile organic compounds have been of particular interest during the past few decades. Studies have shown that after sunset $NO_3\cdot$ has been observed over 100 ppt depending on the environment. It has also been shown that hydrocarbons, particularly isoprene and monoterpenes, are a significant sink of nighttime nitrate radical.

Secondary organic aerosols are formed through the oxidation of various species. Field and laboratory studies have shown that the oxidation of BVOCs by nighttime $NO_3\cdot$ produces SOA. Chamber studies have also been able to observe the first order oxidation of BVOCs, and it is thought that continuing this oxidation will produce significant SOA yields. Of the monoterpenes β-pinene has been labeled the most important of the group in SOA formation.

A field campaign was conducted between August and October of 2016 that measured the trace gases and hydrocarbons in an area north of Houston, TX. The growth of particles was monitored during this time using the CAGE chambers.

Using relevant equations for the production and destruction of $NO_3\cdot$ an equilibrium equation was developed. The trace gases resolved from the trace gas analyzers were put into the developed equilibrium equation and $NO_3\cdot$ was estimated for the length of the field campaign.

Hydrocarbon species were resolved from the PTR-MS and it was determined that the isoprene and monoterpenes were the most active hydrocarbons measured. New

equilibrium equations were developed using the reactions of isoprene and monoterpenes as a sink for NO_3·. Estimated NO_3· was then calculated using the individual hydrocarbons and including both hydrocarbon oxidation reactions.

Estimated SOA yields were calculated using estimated NO_3· and the hydrocarbon measurements. Due to high detection limits and shifting of the PTR-MS during the field campaign, SOA could only be estimated every six hours.

Once estimated, SOA was calculated and growth rates from inside the chamber were compared. It was found that there is some correlation between SOA and growth rates, but the statistics that were run did not show an extremely strong correlation.

5.2. Conclusions

SOA formation has been linked to the oxidation of BVOCs by nighttime nitrate radical. During the field campaign, growth rates of almost 6 nm per hour were observed. The estimated SOA formation was compared to the growth rates observed in the chamber. Some correlation was found, but a strong correlation could not be established.

Reactions, including the destruction of NO_3· by N_2O_5, were ignored during the estimation of NO_3· at the field site. The reactive uptake coefficient of N_2O_5 on real atmospheric particles is highly variable, but when relative humidity is 100% the removal of N_2O_5 by water is elevated. This can create false highs in estimated NO_3·, while truly the amount of NO_3· is much lower. This would result in lower observed growth rates, while the estimated SOA formations are much higher.

Not accounting for the variation in N_2O_5 could be the cause of the lower correlation coefficients between estimated SOA formation and observed growth rates. Having to average the nighttime nitrate radical every six hours could also cause lower correlation coefficients. The natural pattern of the SOA formations is suppressed and only two data points per evenings are available. The large averaging amounts were necessary due to the high detection limits of the monoterpenes and shifting in the PTR-MS. With more data points the correlation between estimated SOA and observed growth rates would likely be higher.

There is some correlation between estimated SOA formation and observed growth rates, and these correlations are significant. The overall pattern of the growth rates greatly resembles that of the estimated SOA formation. The field campaign area had nighttime hydrocarbon measurements of up to 6 ppb. Combined with the nocturnal ozone levels of up to 50 ppb and nocturnal NO and NO_2 levels of up to 15 ppb, there were $NO_3\cdot$ levels up to 25 ppt in the area. All of these conditions are favorable for sizeable SOA formations, and the growth rates observed inside of the chambers provide proof that secondary formation was occurring during this time.

The growth events at night observed inside of the chambers during the field campaign can most likely be attributed to the oxidation of isoprene and monoterpenes by nighttime nitrate radical. To further confirm that these reactions are producing SOA at night, future field campaigns should include more measurements to allow for the calculation of N_2O_5 in the $NO_3\cdot$ concentration estimations. Along with a more sensitive PTR-MS, estimated levels of both $NO_3\cdot$ and SOA could be more accurate. With these

more accurate estimations, the correlation between estimated SOA formation and observed growth rate could be higher. Though the observed particle growth in the area can be attributed to NO_3·-BVOC chemistry, better measurements and more sensitive instrumentation could allow for an even stronger correlation.

REFERENCES

Allan, Beverley J. et al. "The Nitrate Radical in the Remote Marine Boundary Layer." *Journal of Geophysical Research: Atmospheres* 105.D19 (2000): 24191–24204. *CrossRef*. Web.

Atkinson, R. "Atmospheric Chemistry of VOCs and NOx." *Atmospheric Environment* 34.12–14 (2000): 2063–2101. *CrossRef*. Web.

Atkinson, R. "Gas-Phase Tropospheric Chemistry of Volatile Organic Compounds: 1. Alkanes and Alkenes." *Journal of Physical and Chemical Reference Data* 26.2 (1997): 215–290. *CrossRef*. Web.

Atkinson, Roger, and Janet Arey. "Atmospheric Degradation of Volatile Organic Compounds." *Chemical Reviews* 103.12 (2003): 4605–4638. *CrossRef*. Web.

Ayres, B. R. et al. "Organic Nitrate Aerosol Formation via NO_3· + Biogenic Volatile Organic Compounds in the Southeastern United States." *Atmospheric Chemistry and Physics* 15.23 (2015): 13377–13392. *CrossRef*. Web.

Barnes, Ian. et al. "Kinetics and Products of the Reactions of Nitrate Radical with Monoalkenes, Dialkenes, and Monoterpenes." *The Journal of Physical Chemistry* 94.6 (1990): 2413–2419. *CrossRef*. Web.

Berndt, Torsten, and Olaf Böge. "Gas-Phase Reaction of NO_3· Radicals with Isoprene: A Kinetic and Mechanistic Study." *International Journal of Chemical Kinetics* 29.10 (1997): 755–765. *CrossRef*. Web.

Boyd, C. M. et al. "Secondary Organic Aerosol Formation from the β-pinene+NO_3·; System: Effect of Humidity and Peroxy Radical Fate." *Atmospheric Chemistry and Physics* 15.13 (2015): 7497–7522. *CrossRef*. Web.

Brown, S. S., W. P. Dubé, et al. "Biogenic VOC Oxidation and Organic Aerosol Formation in an Urban Nocturnal Boundary Layer: Aircraft Vertical Profiles in Houston, TX." *Atmospheric Chemistry and Physics* 13.22 (2013): 11317–11337. *CrossRef*. Web.

Brown, S. S., J. A. deGouw, et al. "Nocturnal Isoprene Oxidation over the Northeast United States in Summer and Its Impact on Reactive Nitrogen Partitioning and Secondary Organic Aerosol." *Atmospheric Chemistry and Physics* 9.9 (2009): 3027–3042. *CrossRef*. Web.

Brown, Steven S., and Jochen Stutz. "Nighttime Radical Observations and Chemistry." *Chemical Society Reviews* 41.19 (2012): 6405. *CrossRef*. Web.

Carslaw, N. et al. “Simultaneous Observations of Nitrate and Peroxy Radicals in the Marine Boundary Layer.” *Journal of Geophysical Research: Atmospheres* 102.D15 (1997): 18917–18933. *CrossRef*. Web.

Carter, William et al. “Environmental Chamber Study of Maximum Incremental Reactivities of Volatine Organic Compounds.” *Atmospheric Environment* 29.18 (1995): 2499–2511. Print.

Draper, D. C. et al. “A Qualitative Comparison of Secondary Organic Aerosol Yields and Composition from Ozonolysis of Monoterpenes at Varying Concentrations of NO_3” *Atmospheric Chemistry and Physics* 15.21 (2015): 12267–12281. *CrossRef*. Web.

Fan, Jiwen, and Renyi Zhang. “Atmospheric Oxidation Mechanism of Isoprene.” *Environmental Chemistry* 1.3 (2004): 140. *CrossRef*. Web.

Fuentes, Jose D. et al. “Biogenic Hydrocarbon Chemistry within and Above a Mixed Deciduous Forest.” *Journal of Atmospheric Chemistry* 56.2 (2007): 165–185. *CrossRef*. Web.

Fry, J. L., D. C. Draper, et al. “Observations of Gas- and Aerosol-Phase Organic Nitrates at BEACHON-RoMBAS 2011.” *Atmospheric Chemistry and Physics* 13.17 (2013): 8585–8605. *CrossRef*. Web.

Fry, J. L., A. Kiendler-Scharr, A. W. Rollins, P. J. Wooldridge, et al. “Organic Nitrate and Secondary Organic Aerosol Yield from NO_3 Oxidation of β-Pinene Evaluated Using a Gas-Phase Kinetics/Aerosol Partitioning Model.” *Atmospheric Chemistry and Physics* 9.4 (2009): 1431–1449. *CrossRef*. Web.

Fry, J. L., A. Kiendler-Scharr, A. W. Rollins, T. Brauers, et al. “SOA from Limonene: Role of NO_3; in Its Generation and Degradation.” *Atmospheric Chemistry and Physics* 11.8 (2011): 3879–3894. *CrossRef*. Web.

Fry, Juliane L. et al. “Secondary Organic Aerosol Formation and Organic Nitrate Yield from NO_3 Oxidation of Biogenic Hydrocarbons.” *Environmental Science & Technology* 48.20 (2014): 11944–11953. *CrossRef*. Web.

Geyer, Andreas et al. “Chemistry and Oxidation Capacity of the Ntirate Radical in the Continental Boundary Layer near Berlin.” 106.D8 (2001): 8013–8025. Print.

Goldan, P. D., Kuster, W. C., Fehsenfeld, F. C., and Montzka, S. A.: Hydrocarbon measurements in the southeastern United States: The rural oxidants in the southern environment (ROSE) program 1990, J. Geophys. Res.-Atmos., 100, 25945–25963, 1995.

Goldstein, Allen H., and Ian E. Galbally. "Known and Unexplored Organic Constituents in the Earth's Atmosphere." *Environmental Science & Technology* 41.5 (2007): 1514–1521. *CrossRef*. Web.

Gölz, C., J. Senzig, and U. Platt. "NO_3•-Initiated Oxidation of Biogenic Hydrocarbons." *Chemosphere - Global Change Science* 3.3 (2001): 339–352. *CrossRef*. Web.

Griffin, R. J., Cocker, D. R., III, Flagan, R. C., and Seinfeld, J. H.: Organic aerosol formation from the oxidation of biogenic hydrocarbons, J. Geophys. Res., 104, 3555–3567, 1999.

Hallquist, M. et al. "The Formation, Properties and Impact of Secondary Organic Aerosol: Current and Emerging Issues." *Atmospheric Chemistry and Physics* 9.14 (2009): 5155–5236. *CrossRef*. Web.

Heintz, F. et al. "Long-Term Observation of Nitrate Radicals at the Tor Station, Kap Arkona (Rügen)." *Journal of Geophysical Research: Atmospheres* 101.D17 (1996): 22891–22910. *CrossRef*. Web.

Hodzic, A. et al. "Can 3-D Models Explain the Observed Fractions of Fossil and Non-Fossil Carbon in and near Mexico City?" *Atmospheric Chemistry and Physics* 10.22 (2010): 10997–11016. *CrossRef*. Web.

Horowitz, Larry W. et al. "Observational Constraints on the Chemistry of Isoprene Nitrates over the Eastern United States." *Journal of Geophysical Research* 112.D12 (2007): n. pag. *CrossRef*. Web. 4 May 2017.

Hoyle, C. R. et al. "A Review of the Anthropogenic Influence on Biogenic Secondary Organic Aerosol." *Atmospheric Chemistry and Physics* 11.1 (2011): 321–343. *CrossRef*. Web.

Iinuma, Yoshiteru et al. "Evidence for the Existence of Organosulfates from β-Pinene Ozonolysis in Ambient Secondary Organic Aerosol." *Environmental Science & Technology* 41.19 (2007): 6678–6683. *CrossRef*. Web.

Jay, Klaus, and Ludwig Stieglitz. "The Gas Phase Addition of NOx to Olefins." *Chemosphere* 19.12 (1989): 1939–1950. *CrossRef*. Web.

Jimenez, J. L. et al. "Evolution of Organic Aerosols in the Atmosphere." *Science* 326.5959 (2009): 1525–1529. *CrossRef*. Web.

Kiendler-Scharr, A. et al. "Ubiquity of Organic Nitrates from Nighttime Chemistry in the European Submicron Aerosol: Organic Nitrates in European PM1." *Geophysical Research Letters* 43.14 (2016): 7735–7744. *CrossRef*. Web.

Kwok, Eric S. C. et al. “Product Formation from the Reaction of the NO_3· Radical with Isoprene and Rate Constants for the Reactions of Methacrolein and Methyl Vinyl Ketone with the NO_3· Radical.” *International Journal of Chemical Kinetics* 28.12 (1996): 925–934. *CrossRef*. Web.

Ljungström, E., and M. Hallquist. “Nitrate Radical Formation Rates in Scandinavia.” *Atmospheric Environment* 30.16 (1996): 2925–2932. *CrossRef*. Web.

McLaren, Robert et al. “Nighttime Chemistry at a Rural Site in the Lower Fraser Valley.” *Atmospheric Environment* 38.34 (2004): 5837–5848. *CrossRef*. Web.

Magnotta, Frank, and Harold S. Johnston. “Photodissociation Quantum Yields for the NO_3 Free Radical.” *Geophysical Research Letters* 7.10 (1980): 769–772. *CrossRef*. Web.

Mihelcic, D. et al. “Simultaneous Measurements of Peroxy and Nitrate Radicals at Schauinsland.” *Journal of Atmospheric Chemistry* 16.4 (1993): 313–335. *CrossRef*. Web.

Moldanova, J. and Ljungstrom, E.: Modelling of particle formation from NO_3· oxidation of selected monoterpenes, J. Aerosol. Sci., 31, 1317–1333, 2000.

Monks, Paul S. “Gas-Phase Radical Chemistry in the Troposphere.” *Chemical Society Reviews* 34.5 (2005): 376. *CrossRef*. Web.

Nah, Theodora et al. “Influence of Seed Aerosol Surface Area and Oxidation Rate on Vapor Wall Deposition and SOA Mass Yields: A Case Study with Alpha-Pinene Ozonolysis.” *Atmospheric Chemistry and Physics* 16.14 (2016): 9361–9379. *CrossRef*. Web.

Ng, N. L. et al. “Secondary Organic Aerosol (SOA) Formation from Reaction of Isoprene with Nitrate Radicals (NO_3).” *Atmospheric Chemistry and Physics* 8.14 (2008): 4117–4140. *CrossRef*. Web.

Ng, Nga Lee et al. “Nitrate Radicals and Biogenic Volatile Organic Compounds: Oxidation, Mechanisms, and Organic Aerosol.” *Atmospheric Chemistry and Physics* 17.3 (2017): 2103–2162. *CrossRef*. Web.

Noxon, J. F., R. B. Norton, and W. R. Henderson. “Observation of Atmospheric NO_3.” *Geophysical Research Letters* 5.8 (1978): 675–678. *CrossRef*. Web.

Orlando, John J. et al. “Quantum Yields for Nitrate Radical Photolysis between 570 and 635 Nm.” *The Journal of Physical Chemistry* 97.42 (1993): 10996–11000. *CrossRef*. Web.

Penkett, S. A. et al. “The Seasonal Variation of Nonmethane Hydrocarbons in the Free Troposphere over the North Atlantic Ocean: Possible Evidence for Extensive Reaction of Hydrocarbons with the Nitrate Radical.” *Journal of Geophysical Research: Atmospheres* 98.D2 (1993): 2865–2885. *CrossRef*. Web.

Penkett, S.A. et al. “Evidence for Large Average Concentrations of the Nitrate Radical (NO_3·) in Western Europe from the HANSA Hydrocarbon Database.” *Atmospheric Environment* 41.16 (2007): 3465–3478. *CrossRef*. Web.

Perraud, V., Bruns, E. A., Ezell, M. J., Johnson, S. N., Greaves, J., and Finlayson-Pitts, B. J.: Identification of organic nitrates in the NO_3· radical initiated oxidation of α-pinene by atmospheric pressure chemical ionization mass spectrometry, Environ. Sci. Technol., 44, 5887–5893, 2010.

Platt, U., G. LeBras, et al. “Peroxy Radicals from Night-Time Reaction of N03 with Organic Compounds.” *Nature* 348.6297 (1990): 147–149. *CrossRef*. Web.

Platt, U., D. Perner, et al. “The Diurnal Variation of NO $_3$.” *Journal of Geophysical Research* 86.C12 (1981): 11965. *CrossRef*. Web.

Platt, Ulrich et al. “Detection of NO $_3$ in the Polluted Troposphere by Differential Optical Absorption.” *Geophysical Research Letters* 7.1 (1980): 89–92. *CrossRef*. Web.

Pye, H. O. T. et al. “Global Modeling of Organic Aerosol: The Importance of Reactive Nitrogen (NO_x and NO_3).” *Atmospheric Chemistry and Physics* 10.22 (2010): 11261–11276. *CrossRef*. Web.

Rastogi, Neeraj et al. “Filterable Water-Soluble Organic Nitrogen in Fine Particles over the Southeastern USA during Summer.” *Atmospheric Environment* 45.33 (2011): 6040–6047. *CrossRef*. Web.

Rollins, A. W. et al. “Evidence for NOx Control over Nighttime SOA Formation.” *Science* 337.6099 (2012): 1210–1212. *CrossRef*. Web.

Schichtel, Bret A. et al. “Fossil and Contemporary Fine Particulate Carbon Fractions at 12 Rural and Urban Sites in the United States.” *Journal of Geophysical Research* 113.D2 (2008): n. pag. *CrossRef*. Web. 21 Apr. 2017.

Skov, H. et al. “Products and Mechanisms of the Reactions of the Nitrate Radical (NO_3·) with Isoprene, 1,3-Butadiene and 2,3-Dimethyl-1,3-Butadiene in Air.” *Atmospheric Environment. Part A. General Topics* 26.15 (1992): 2771–2783. *CrossRef*. Web.

Smith, Nicola et al. “Nighttime Radical Chemistry in the San Joaquin Valley.” *Atmospheric Environment* 29.21 (1995): 2887–2897. *CrossRef*. Web.

Spittler, M., Barnes, I., Bejan, I., Brockmann, K. J., Benter, T., and Wirtz, K.: Reactions of NO_3· radicals with limonene and alphapinene: Product and SOA formation, Atmos. Environ., 40, S116– S127, 2006.

Stutz, Jochen et al. “Nocturnal NO_3· Radical Chemistry in Houston, TX.” *Atmospheric Environment* 44.33 (2010): 4099–4106. *CrossRef*. Web.

Suh, Inseon, Wenfang Lei, and Renyi Zhang. “Experimental and Theoretical Studies of Isoprene Reaction with NO $_3$.” *The Journal of Physical Chemistry A* 105.26 (2001): 6471–6478. *CrossRef*. Web.

von Kuhlmann, R. et al. “Sensitivities in Global Scale Modeling of Isoprene.” *Atmospheric Chemistry and Physics* 4.1 (2004): 1–17. *CrossRef*. Web.

Wayne, R.P et al. “The Nitrate Radical: Physics, Chemistry, and the Atmosphere.” *Atmospheric Environment. Part A. General Topics* 25.1 (1991): 1–203. *CrossRef*. Web.

Winer, A. M., R. Atkinson, and J. N. Pitts. “Gaseous Nitrate Radical: Possible Nighttime Atmospheric Sink for Biogenic Organic Compounds.” *Science* 224.4645 (1984): 156–159. *CrossRef*. Web.

Xie, Y. et al. “Understanding the Impact of Recent Advances in Isoprene Photooxidation on Simulations of Regional Air Quality.” *Atmospheric Chemistry and Physics* 13.16 (2013): 8439–8455. *CrossRef*. Web.

Zhang, Dan, and Renyi Zhang. “Unimolecular Decomposition of Nitrooxyalkyl Radicals from NO_3·–isoprene Reaction.” *The Journal of Chemical Physics* 116.22 (2002): 9721–9728. *CrossRef*. Web.

Zhang, Q. et al. “Ubiquity and Dominance of Oxygenated Species in Organic Aerosols in Anthropogenically-Influenced Northern Hemisphere Midlatitudes: UBIQUITY AND DOMINANCE OF OXYGENATED OA.” *Geophysical Research Letters* 34.13 (2007): n/a-n/a. *CrossRef*. Web.

Zhang, R. “Getting to the Critical Nucleus of Aerosol Formation.” *Science* 328.5984 (2010): 1366–1367. *CrossRef*. Web.